Challenges of Crystal Structure Prediction of Diastereomeric Salt Pairs

Panagiotis G. Karamertzanis and Sarah L. Price*

Department of Chemistry, University College London, 20 Gordon Street, London WC1H 0AJ, United Kingdom

Received: May 11, 2005; In Final Form: July 12, 2005

A methodology for the computational prediction of the crystal structures and resolution efficiency for diastereomeric salt pairs is developed by considering the polymorphic system of the diastereomeric salt pair (*R*)-1-phenylethylammonium (*R*/*S*)-2-phenylpropanoate. To alleviate the mathematical complexity of the search for minima in the lattice energy due to the presence of two flexible entities in the asymmetric unit, the range of rigid-body lattice energy global optimizations was guided by a statistical analysis of the Cambridge Structural Database for common ion-pair geometries and ion conformations. A distributed multipole model for the dominant electrostatic interactions and high-level ab initio calculations for the intramolecular energy penalty for conformational distortions are used to quantify the relative stabilities of the p- and n-salt forms. While the ab initio prediction of the known structure of the p-salt as the most stable structure was insensitive to minor changes in the rigid-ion conformations considered, the relative stabilities of the known polymorphs and hypothetical structures of the n-salt were very sensitive. Although this paper provides a significant advance over traditional search algorithms and empirical force fields in determining the structures and relative stabilities of diastereomeric salt pairs, the sensitivity of the computed lattice energies to the fine details of the ion conformations overtaxes current computational models and renders the design of diastereomeric resolution processes by computational chemistry a challenging problem.

1. Introduction

A methodology for the prediction of the thermodynamic relative stability of diastereomeric salt pairs would have an immense impact on the manufacture of chemical entities in optically pure form when stereoselective synthesis or isolation from natural products are not feasible, as it will assist the design of separation processes based on diastereomeric resolution. The majority of racemic mixtures (90−95% of the cases, if not more due to the underestimation of the actual proportion due to a bias) crystallize in racemic crystals.[1−3] This trend can be attributed to the additional possibilities for favorable packing when both enantiomers are present, though the racemate may also be preferred kinetically when the growth of the nuclei of a chiral crystal is inhibited by the attachment of molecules of opposite chirality.[4] When spontaneous resolution (preferential crystallization) is not feasible, chiral resolution can often be accomplished via the addition of a chiral resolving agent, typically in the form of an optically pure acid or base, which leads to the one of the two diastereomeric salts being selectively crystallized.

Diastereomeric salt formation was initially applied by Pasteur as early as 1853[5] and is currently one of the preferred methods for resolutions on an industrial scale.[6] It is based on the fact that although the enantiomers have the same physical properties the resulting diastereomeric salts often exhibit dissimilar physicochemical properties, such as melting points, enthalpies of fusion, and solubilities. This difference in solubility can lead to differential crystallization and thus is an important determinant of the resolution efficiency. To date there is no established methodology for the prediction of the optimal resolving agent for a given racemic substrate.[7,8] The design of the separation process usually involves the experimental screening of a set of resolving agents with the aim to identify the one that achieves the highest diastereomeric excess and chemical yield.[2,8−13] Quite often the devised resolution process achieves suboptimal resolvabilities due to the lack of time for screening enough resolving agents despite their limited number.[7]

Thermodynamic considerations show that the resolution ability—expressed as $\ln(c_p/c_n)$ where c_p and c_n are the solubilities of the p- and n-salts respectively—is proportional to the solid-state free energy differences if there is no interionic interaction in solution[14] (i.e., assuming complete dissociation and solvation). As current computational models are rapidly progressing toward the reliable calculation of lattice energies[15] and estimates of free energies[16,17] (at least within the harmonic approximation) of solids, this raises the possibility of computationally screening candidate resolving agents on the basis of the calculated relative energies of the p- and n-salt. This requires the reliable prediction of the structures and relative energies of the crystals of the diastereomeric salt pair.

The field of computational crystal structure prediction is rapidly evolving because of its potential benefits in the design of new molecular materials and in aiding the screening of pharmaceuticals for polymorphism. Most of the methods that had some success in the blind tests of crystal structure prediction[18,19] are based on searching through the vast phase space of possible space groups, lattice vectors, and molecular positions for structures for energetically competitive minima in the lattice energy. Even for molecules that can be treated as rigid and adopt structures with only one molecule in the asymmetric unit, this approach usually generates significantly more hypothetical structures that are thermodynamically plausible than known polymorphs. Extending this methodology to salts unfortunately makes the mathematical complexity of the search for low-lattice-energy crystal structures overwhelming,

* Author to whom correspondence should be addressed. E-mail: s.l.price@ucl.ac.uk

10.1021/jp052465n CCC: $30.25
Published on Web 08/23/2005

because of the presence of two molecular entities in the asymmetric unit. The difficulty is compounded by the fact that chiral entities are often flexible, and hence the search has to consider conformational changes in which the intramolecular energy penalty for a conformational change may be compensated for by improved lattice energy. This requires that the intra- and intermolecular energy of the hypothetical p- and n-salt structures should be computed with sufficient accuracy to allow a reliable prediction of their relative stabilities. Thus, although the potential of computational crystal structure prediction to be used for screening of resolving agents has long been recognized,[14,20] there have been few previous attempts to model and predict the solid state of organic salts.[21−23]

A study of a wide range of pharmaceutical-type compounds has clearly shown that the limitations of empirical atom−atom intramolecular force fields often lead to significant distortions of the molecular conformation[24] and hence prevent the accurate modeling of the crystal structure. A study of organometallic salts[25] also demonstrated that polymorph prediction may be severely hampered by even small inaccuracies in the molecular structures, suggesting that the effects of conformational inaccuracies may be amplified when dealing with charged molecular entities. Combining an accurate ab-initio-based, anisotropic, polarizable model for the intermolecular interactions[26,27] with ab initio conformational energies allowed the reliable reproduction of the known crystal geometries of glycol,[28] glycerol,[28] and a set of six monosaccharides[29] and improved their ranking over empirical force fields. However, although these highly accurate models represent a significant improvement over empirical atom−atom force fields, their extension to the crystal structure prediction of salts is computationally prohibitive due to the presence of two molecular entities. In this work, we introduce an alternative methodology based on a high-level ab initio exploration of the conformational space, complemented by a statistical analysis of the Cambridge Structural Database[30] (CSD) for statistically favored conformations. This allows the consideration of a small set of probable, low-energy molecular ion geometries that are held rigid throughout the search for low-lattice-energy crystal structures.[31] Even when no intramolecular degrees of freedom are considered, the presence of two molecular entities in the asymmetric unit increases the number of possible crystal structures and hence the computational cost.[32] Thus, in this paper, candidate crystal structures were systematically generated via the application of common proper symmetry operations on a set of suitably chosen ion-pair clusters. The relative position and orientation of the two ions in the cluster were varied, by considering geometries of high probability derived from a statistical analysis of the CSD, to ensure that a sufficiently large number of starting points for lattice energy minimization was generated. The relative lattice energies of the hypothetical structures were computed with an accurate distributed multipole model for the dominant electrostatic interactions. The efficient exploration of the energy surface for crystals with more than one molecular entity in the asymmetric unit, along with improvements in the accuracy of both intra- and intermolecular contributions to the lattice energy, are the main contributions of this paper to the algorithms for crystal structure prediction.[18,19,33]

The methodology is applied in the case of the diastereomeric salt pair [1]-1-phenylethylammonimum [2]-2-phenylpropanoate, shown in Figure 1, for which both the p-salt ([1]-*R*, [2]-*S* or [1]-*S*, [2]-*R*) and the n-salt structures ([1]-*R*, [2]-*R* or [1]-*S*, [2]-*S*) have been determined by means of single-crystal X-ray diffraction.[34,35] Studies with the ternary system consisting of the p- and n-salt and ethanol revealed that these salts crystallize as a eutectic mixture with the p-salt being less soluble[36] and therefore more thermodynamically stable at room temperature. This agrees with the inference from the n-salt having a lower melting point and heat of fusion.[37] The n-salt undergoes a phase transition on heating at 104.7 °C (n-salt I → n-salt II), which has been confirmed by temperature-resolved X-ray powder diffraction (XRPD).[37] The polymorphic landscape of this system has been further enriched by the discovery of an unstable racemic compound produced during the rapid crystallization of a [1]-*R*,*S* and [2]-*R*,*S* solution by fast cooling or solvent evaporation.[37] The latter racemic form and the high-temperature n-salt form (n-salt II) have recently been analyzed by single-crystal X-ray diffraction.[38] The wealth of high-quality single-crystal determinations along with the solid evidence on the relative stability of the various forms makes this system a challenging case for validating theoretical prediction methodology.

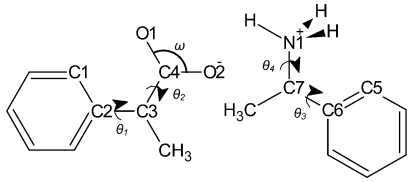

Figure 1. Molecular structures of 2-phenylpropanoate (left) and 1-phenylethylammonium (right). The effects of the rotation of the phenyl θ_1 (torsion angle C1−C2−C3−C4) and θ_3 (N1−C7−C6−C5), carboxylate θ_2 (O1−C4−C3−C2), and ammonium θ_4 (H1−N1−C7−C6) groups around the chiral centers and the distortion of the carboxylate angle ω (O1−C4−O2) in the modeling of the known forms and crystal structure prediction have been investigated.[94]

2. Methodology

The first step of the proposed algorithm for crystal structure prediction of diastereomeric salts is a conformational analysis to identify the range of low-energy molecular conformations of the ions that can appear in the solid state. Suitable sets of rigid-ion conformers are used in the construction of many ion-pair clusters by altering the relative position and orientation of the two ions to sample the most probable hydrogen-bond geometries determined from a statistical analysis of the CSD. The ion-pair clusters are subsequently used as building blocks to construct a large number of dense candidate crystal structures via the application of statistically common symmetry operations within chiral space groups. All candidate crystal structures are refined by lattice energy minimization, and the unique minima that are energetically plausible are considered for further analysis.

To validate the modeling methodology, we have performed lattice energy minimizations of the known crystal forms. In particular, we established the sensitivity of their predicted intermolecular energies and geometric reproduction to the packing-induced distortions of the ion conformations and hence how well the rigid-body search approach can be expected to predict the experimental data. This section focuses on each of the aforementioned steps of the search algorithm and validation procedure in more detail.

2.1. Conformational Analysis. To assess the relative stability of the known crystal structures it is necessary to consider the differences in the intramolecular energy due to the distortion of the gas-phase conformations of the two ions under the packing forces. Unfortunately, the experimentally determined molecular conformations cannot be used directly in ab initio calculations because the intramolecular energy estimates will

be dominated by experimentally insignificant errors in the bond lengths and angles. Thus, before the intramolecular energy differences are estimated, the experimental conformations are partially ab initio minimized by constraining all "soft" internal degrees of freedom to their experimental values. The set of soft degrees of freedom comprise the internal coordinates whose value can be significantly affected by the packing forces within the crystal. This definition implies that there is a threshold of stiffness, above which the value of an internal degree of freedom is considered to be unaffected by the intermolecular interactions; i.e., it will be the same in the crystalline and the gas phases. Although bond lengths are generally accepted to be above any reasonably chosen threshold, this is not always true for bond angles and definitely not true for many torsion angles involving single bonds. Thus, the classification of the internal degrees of freedom as soft or hard modes relies on chemical intuition, with gray areas leading to difficulties in the estimation of the differences of the intramolecular energies (and thus the lattice energies) between conformational polymorphs.

For the salt system in this study, we considered the effect of the rotation of the phenyl (torsion θ_1) and carboxylate (torsion θ_2) groups for the anion and the rotation of the phenyl (torsion θ_3) and ammonium (torsion θ_4) groups for the cation (Figure 1). The molecular conformations and corresponding intramolecular energies were calculated with a 6-31G(d,p) basis set with frozen inner cores, corrected for the effect of electron correlation via Möller−Plesset perturbation expansion of the second order within the suite of electronic structure programs Gaussian.[39] The results of the gas-phase calculations were contrasted to statistical evidence from data extracted from the CSD using the program MOGUL[40] to identify all crystal structures that contained 1-phenylethylammonimum or 2-phenylpropanoate fragments.

In an ab initio crystal structure prediction framework for flexible molecules and ions, we seek to identify the crystal structures of lowest total lattice energy $\Delta E + U$, where ΔE is the intramolecular energy penalty for conformational distortions from the ab initio global minimum (in vacuo conformation), and U the intermolecular lattice energy. In principle, this implies that we need to consider all conformations with intramolecular energy penalty ΔE sufficiently small that it could be compensated for by favorable intermolecular interactions. However, due to the computational cost associated with the rigid-body search for each set of ion conformations, we considered the ab initio and statistical information on the range of possible conformations prior to selecting only a few ion conformations for use in the search.

2.2. Construction of Ion Probes and Candidate Crystal Structures. The generation of initial crystal structures for lattice energy minimization of salts for a worthwhile search needs to be efficient and to use crystallographic insight because of the computational cost of performing large numbers of lattice energy minimizations. Treating the two ions independently and building candidate crystal structures by positioning the ions randomly or systematically will lead to a huge proportion of minimizations that will be unable to reach low-energy minima because the carboxylate and ammonium groups may remain at long distances and/or unfavorable relative orientations. Thus, we first construct sets of ion-pair clusters in probable geometries and then systematically generate dense packings within common crystallographic coordination environments.

The exact position of the center of mass and Euler angles of the two ions in the candidate structures are not critical because their relative position and orientation will be relaxed during the lattice energy minimization. However, the preset geometry of the ion-pair cluster during the generation of candidate crystals may restrict the accessible lattice energy space, particularly since the generated candidate structures have a high density that prevents significant packing rearrangements. Thus, for a given set of molecular conformations and to ensure a reasonably extensive search, it is necessary to consider a sufficiently large number of cluster geometries for crystal structure prediction. Thus, in this study we opted to construct a set of ion-pair clusters of predefined geometries, to represent the range that appears frequently in the CSD, and use the latter as building blocks for the generation of candidate crystal structures.

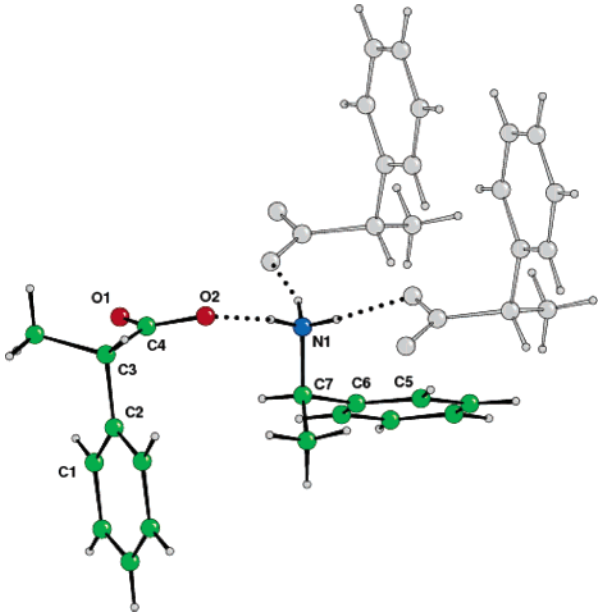

Figure 2. Hydrogen-bonded coordination environment of the experimentally determined p-salt containing a (*R*)-1-phenylethylammonium cation hydrogen-bonded to three (*S*)-2-phenylpropanoate anions. The ion pair in black constitutes an example ion-pair cluster, whose geometry is defined by the distance $\delta_{N1\cdots O2}$, the angles $\omega_{C7N1\cdots O2}$ and $\omega_{N1\cdots O2C4}$, and the torsion angles $\phi_{C6C7N1\cdots O2}$, $\phi_{C7N1\cdots O2C4}$, and $\phi_{N1\cdots O2C4C3}$. Due to the presence of multiple hydrogen-bonded donors and acceptors, this set of variables and their values are not unique.

The geometry of a pair of molecular ions of specified conformation is defined on the basis of one length, two angles, and three torsion angles between two sets of three noncollinear atoms belonging to each of the molecular entities. In cases such as diastereomeric salt pairs, where the occurrence of strong hydrogen bonds between the oppositely charged groups is inevitable, it is more effective to choose atoms in the vicinity of the hydrogen-bond donor and acceptor. In this work, the relative position and orientation of the ion pair was defined via the set of variables $\delta_{N1\cdots O2}$, $\omega_{C7N1\cdots O2}$, $\phi_{C6C7N1\cdots O2}$, $\omega_{N1\cdots O2C4}$, $\phi_{C7N1\cdots O2C4}$, and $\phi_{N1\cdots O2C4C3}$ (Figure 2). Plausible hydrogen-bonding geometries were generated by focusing on the hydrogen-bonded motifs of similar compounds retrieved from the CSD (version 5.25, November 2003). The set of similar compounds was identified by selecting all organic crystal structures for which the pair of ions $RCCNH_3^+$ and $RCCOO^-$ was present (Figure 3), without imposing a limit on the number of such pairs per asymmetric unit, but excluding crystals containing other ions. All entries that were polymeric, erroneous, or containing atoms with undetermined positions were also excluded. The duplicate structures were eliminated by retaining only the most accurate determination based on a comparison of the *R*-factors, the radiation source (X-ray or neutron scattering), and the temperature of data collection.

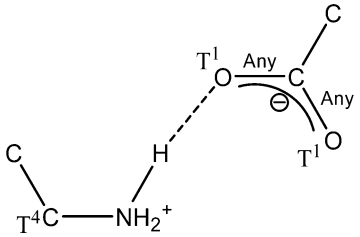

Figure 3. CSD search moiety used to investigate the range of ion-pair geometries. T^k denotes a *k*-coordinated atom.

After the CSD analysis and after testing that the ion-pair clusters were different enough to ensure that the majority of the corresponding candidate structures do not converge to the same minimum, we considered on average 20−30 probable cluster geometries per set of molecular conformations. Each ion-pair cluster considered is replicated in space through the application of symmetry operations by MOLPAK,[41] to obtain candidate crystal structures for lattice energy minimization. The latter are dense structures constructed via a grid search on the orientations of the ion-pair cluster in the nine most common coordination environments belonging to the chiral space groups $P1$, $P2_1$, $P2_12_12$, $P2_12_12_1$, and $C2$. Ideally, all 65 space groups that contain only proper symmetry operations should be considered; however, a statistical analysis[3,42,43] of the CSD reveals that the considered subset of chiral space groups contains all those that occur predominantly for asymmetric molecules. Preliminary studies showed that up to 125 such structures per MOLPAK coordination environment should be considered to allow a thorough exploration of the lattice energy surface for the specific packing type without an excessively large number of initial points converging to the same minimum.

The search for low-energy crystal structures was performed on a Beowulf cluster using a recently developed Grid computational service.[44] Initially, the generation of candidate crystals for one ion-pair geometry in the nine chiral MOLPAK packing types is distributed to an equal number of nodes. Then, local lattice energy minimization jobs are distributed to as many as 90 nodes, and the results are gathered into one database. The parallelization of the search allows a full MOLPAK/DMAREL run that involves up to 1125 minimizations to be completed in approximately 3 h. The reported results were produced after approximately 200 such searches. The low-energy p- and n-salt hypothetical crystal structures for the search with the CSD-derived ion conformations are available upon request from the authors.

2.3. Modeling of Intermolecular Interactions and Local Lattice Energy Minimization Algorithm. The repulsion−dispersion contribution to the lattice energy has the form

$$U_{12}^{\text{rep-dis}} = \sum_{i\in 1}\sum_{k\in 2}(A_{\iota}A_{\kappa\kappa})^{1/2}\, e^{-(B_{\iota}+B_{\kappa\kappa})R_{\iota\kappa}/2} - \frac{(C_{\iota}C_{\kappa\kappa})^{1/2}}{R_{ik}^{\,6}}$$

where atom i in molecule 1 is of type ι and atom k in molecule 2 of type κ. The parameters for the atomic types C, N, O, and H_C (hydrogen connected to carbon) were taken from Williams[45,46] and for H_N (hydrogen connected to nitrogen) from a reparametrization of this force field to model hydrogen-bonded crystals in conjunction with an accurate electrostatic model based on atomic multipoles[47] (Table 1). The electrostatic interactions were modeled via a set of atomic multipoles calculated from a distributed multipole analysis of the MP2/6-31G(d,p) charge density[48,49] using all terms up to hexadecapole. The contributions from the slowly convergent multipole−multipole energy terms, corresponding to the charge−charge, charge−dipole, and dipole−dipole interactions, were calculated with the Ewald summation[50] technique. All higher-order electrostatic interactions, up to R^{-5}, were summed to a 15-Å cutoff distance between the centers of mass of the molecules.

TABLE 1: Repulsion−Dispersion Potential Parameters Used in Conjunction with a Distributed Multipole Electrostatic Model Derived from the MP2/6-31G(d,p) Charge Densities of the Isolated Ions[a]

interaction	A (kJ mol^{-1})	B (Å^{-1})	C (kJ mol^{-1} Å^6)
C···C	369 746	3.60	2439.8
N···N	254 531	3.78	1378.4
O···O	230 066	3.96	1123.6
H_C···H_C	11 971	3.74	136.4
H_N···H_N	5030	4.66	21.5

[a] All parameters were derived by fitting in combination with a point charge model apart from the polar hydrogen interactions (H_N···H_N) that were derived by fitting in combination with a distributed multipole model.[45−47]

The lattice energy minimization was performed by DMAREL[51] within the space group constraints, and thus the obtained minima may correspond to saddle points once the symmetry constraints are removed. The detection of saddle points was accomplished via the examination of the second derivative matrix for negative eigenvalues or the presence of unstable elastic constants and/or imaginary phonon frequencies. (Structures that are unstable to cell doubling will not be detected by our phonon frequency calculations[16] that are currently restricted to $\mathbf{k} = 0$.) It was not attempted to repeat the minimization with the corresponding symmetry representation of the space group removed, and such saddle points were discarded, because the search for structures with more than one anion and cation pair in the asymmetric unit is beyond the scope of this study.

In many cases, apparently different minima correspond to essentially the same crystal structure although their unit cells are expressed with different choices of axes. Duplicates were discarded following comparison of the Niggli reduced cell parameters[52−55] (as calculated by PLATON[56]), lattice energies and densities, the simulated powder X-ray patterns (by applying a recently published algorithm relying on the calculation of cross-correlation functions[57]), and the interatomic distances in the molecular coordination sphere.[58] The latter two methods form a complementary analysis that avoids the use of the space group and cell information and can identify similarities of structures in different settings without involving transformations.[59] The unique low-energy crystal structures were visualized using Mercury,[60] and their hydrogen-bond patterns were characterized using graph set analysis.[61,62]

3. Results

3.1. Conformational Analysis. The one-dimensional intramolecular energy variation for the rotation of the phenyl groups for the anion $\Delta E(\theta_1)$ and the cation $\Delta E(\theta_3)$ are shown in Figure 4. The cation has only one conformational minimum, while the anion exhibits two such minima; the global minimum corresponds to $\theta_1 = 49.56°$ and is 3.19 kJ mol^{-1} more stable than the second minimum obtained at $\theta_1 = 117.68°$. For the anion, the rotation of the phenyl group by 180° around the C2−C3 axis (θ_1) leads to large variations in the rotation of the carboxylate group around the C4−C3 axis (θ_2). However, in the case of the cation, the rotation of the ammonium group around the N1−C7 axis (θ_4) is less dependent on the rotation of the phenyl group (θ_3) and varies by less than 20°.

The two-dimensional intramolecular energy surfaces for the anion, $\Delta E(\theta_1, \theta_2)$, and the cation, $\Delta E(\theta_3, \theta_4)$, in the range of

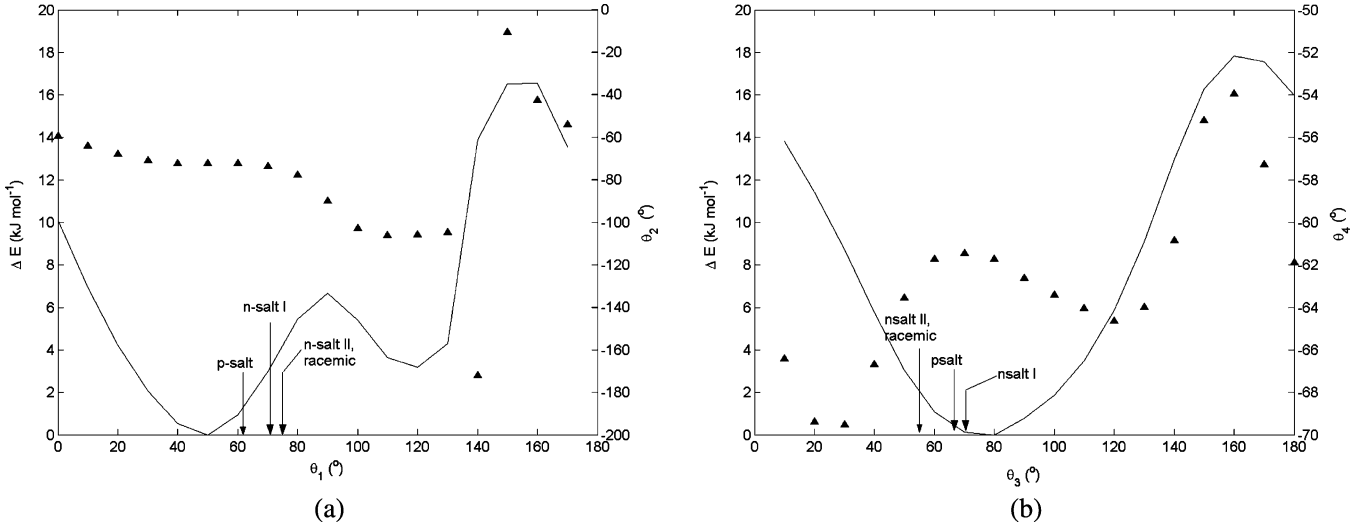

Figure 4. Relaxed scan ΔE for the phenyl group rotation for (a) (*R*)-2-phenylpropanoate and (b) (*R*)-1-phenylethylammonium at the MP2/6-31G-(d,p) level of theory. The intramolecular energy is shown as a black continuous line on the left vertical axes. (a) The rotation of the carboxylate group, torsion θ_2, around the C4−C3 bond and (b) the rotation of the ammonium group, torsion θ_4, around the N1−C7 bond at the minima are shown as blue triangles on the right vertical axes.

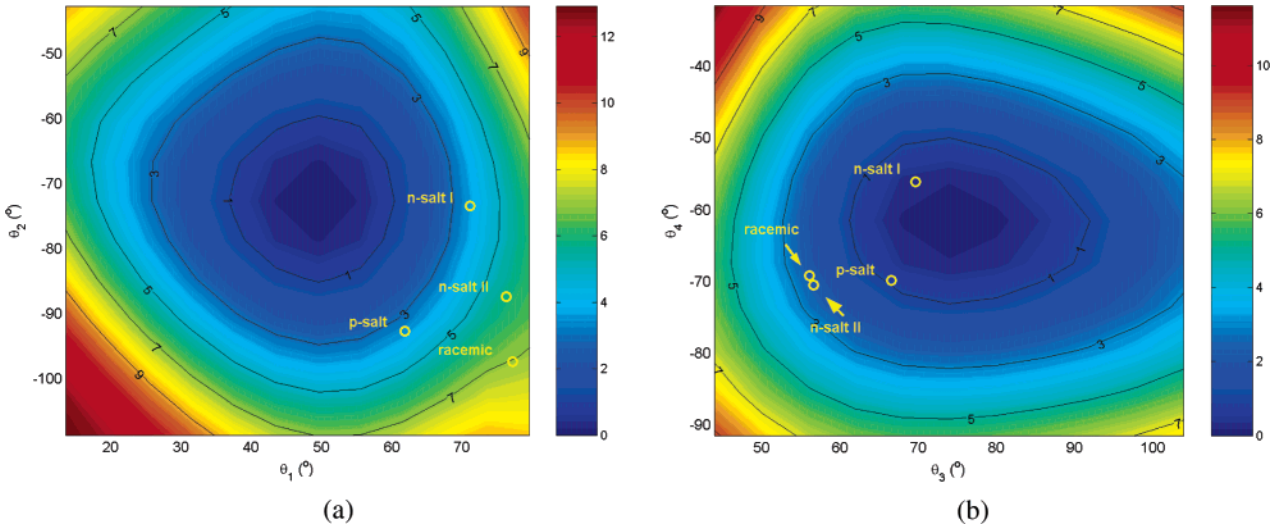

Figure 5. Two-dimensional relaxed scan ΔE (in kJ mol^{-1}) for (a) (*R*)-2-phenylpropanoate and (b) (*R*)-1-phenylethylammonium in the region around the conformational global minima at the MP2/6-31G(d,p) level of theory. Circles correspond to the experimentally determined molecular conformations. (The torsion angles for [1]-*S* and [2]-*S* were inverted to refer to their chiral counterparts.[94])

torsion angles around the global minima are shown in Figure 5. It is evident that all θ_1, θ_2, θ_3, and θ_4 torsions can differ by up to 30° from their unconstrained optimized values without incurring a significant increase in the intramolecular energy relative to the large lattice energies of ionic systems, confirming the assumption that the ion conformations may be significantly affected by the packing forces. As demonstrated in the Supporting Information, it is essential to calculate the energy penalties ΔE at the MP2 level, though a considerable saving in computer time could have been achieved by optimizing the geometries at the self-consistent field (SCF) level.[63,64] From the ab initio calculations, we estimate that the intramolecular energy due to the effects of the packing forces on the rotation of the phenyl and ammonium groups of the cation does not exceed 2.3 kJ mol^{-1} in any observed crystal structure. However, the distortions due to the rotation of the phenyl and carboxylate groups of the anion are characterized by higher intramolecular energies that become equal to 5.9 and 7.1 kJ mol^{-1} in the case of the n-salt II and racemic form, respectively. These are small energies compared with the lattice energies of the salts. It is, however, notable that the ion geometries found in all the experimentally determined crystal structures are clustered in a narrow region of conformational space, suggesting that the effects of the packing forces on the ion conformations may be systematic.

Hence, the variation in the rotation of the phenyl and carboxylate groups in 1-phenylethylammonium and 2-phenylpropanoate fragments in experimental crystal structures from the CSD (Figure 6) was contrasted with the ab initio intramolecular energy calculations in Figures 4 and 5. The conformations found in the crystal structures congregate in the proximity of low-energy wells with only a few crystal structures containing phenyl group rotations, which have an intramolecular strain exceeding 5 kJ mol^{-1}, as found in previous studies on the complementarity of statistical and quantum mechanical conformational analyses for other systems.[65] In the case of 2-phenylpropanoate, the probability distribution (Figure 6a) for the rotation of the phenyl group exhibits a strong peak at $\theta_1 = 75°$, which is asymmetric with more structures between 45° and 75° than between 75° and 105°. The CSD survey showed that the phenyl and methyl groups at an eclipse configuration ($\theta_3 \approx 120°$) are not statistically probable, although the intramolecular

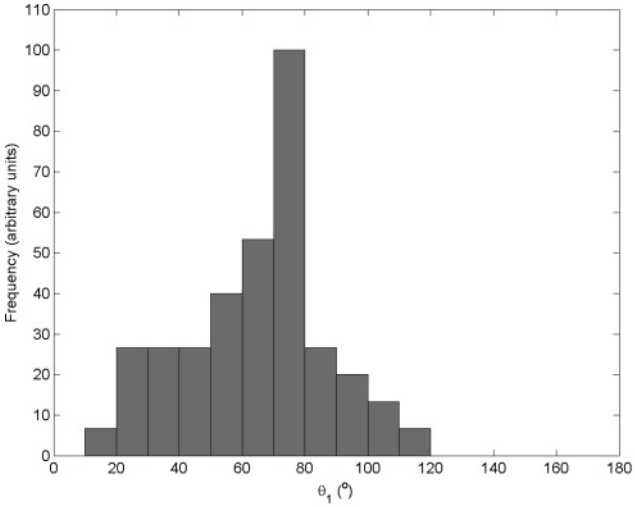

(a) phenyl rotation in 2-phenylpropanoate

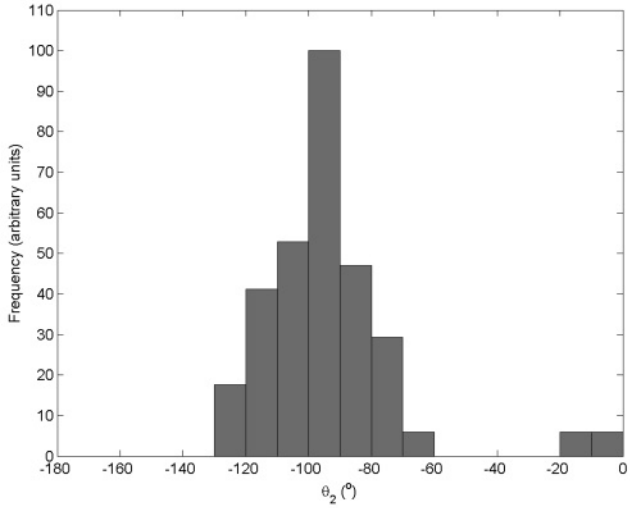

(b) carboxylate rotation in 2-phenylpropanoate

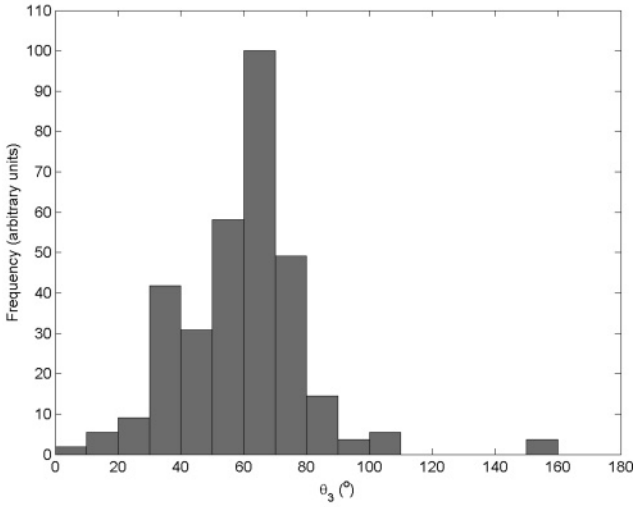

(c) phenyl rotation in 1-phenylethylammonium

Figure 6. Histograms for the rotation of the (a) phenyl and (b) carboxylate groups in 2-phenylpropanoate and (c) the phenyl group in 1-phenylethylammonium fragments found in crystal structures in the CSD (52 and 178 unique molecular conformations with *R*-factor ≤7.5%, respectively. (The torsion angles for [1]-*S* and [2]-*S* were inverted to refer to their chiral counterparts.[94])

energy surface exhibits a local minimum (Figure 4a) that is only 3.19 kJ mol^{-1} less stable than the conformational global minimum. The rotation of the carboxylate group (θ_2) around the bond C4−C3 (Figure 6b) exhibits a strong peak around the average value of −94.30°, which is significantly different from the ab-initio-optimized value of −72.68°. In agreement with earlier statistical evidence,[66] in the majority of 1-phenylethylammonium fragments the rotation of the phenyl group corresponds to θ_3 values in a narrow region around the average value of 59.75° (Figure 6c) and not around the conformational minimum at 73.98°. The peak was asymmetric with the majority of the structures having torsion θ_3 smaller than the value at the intramolecular energy minimum (Figure 4b), i.e. there are fewer conformations to the side of the well with the phenyl ring closer to the CH_3 group. Thus, we can speculate that in the case of the cation the intermolecular interactions compensate for the increase in intramolecular energy when the phenyl ring rotation is between 30° and the ab initio minimum, probably because these conformations facilitate the formation of energetically favorable hydrogen bonds. On the basis of the results of the conformational analysis, the conformational global minima (in vacuo) and the statistical average conformations (CSD conformations hereafter) of both ions, corresponding to the ab-initio-optimized ion conformations under the constraints $\theta_1 = 64.89°$, $\theta_2 = -94.30°$, and $\theta_3 = 59.75°$, were considered in crystal structure prediction studies for both the p- and n-salts.

3.2. Modeling of Experimental Crystal Structures. *3.2.1. Analysis of Available Crystal Structures.* The hydrogen-bonding patterns in all experimentally determined forms exhibit similarities with the ammonium group of the cation hydrogen-bonded to the carboxylate group of three anions and one of the oxygen atoms of the carboxylate group acting as an acceptor to two ammonium groups. All known forms contain infinite hydrogen-bonded ladder-shaped chains[38] comprised of rings sharing one N−H···O edge. However, in the case of the enantiomorphous salts, the chains result from the arrangement of ions along 2_1 screw axes, forming R_4^3 (10) rings contrasting with the arrangement of the ions in the chains of the racemic compound that are related by inversion centers forming alternating R_4^2 (8) and R_4^4 (12) rings. Despite these similarities, the ion-pair clusters differ, particularly in the torsion angles $\phi_{CN\cdots OC}$ and $\phi_{N\cdots OCC}$ (Table S1 in the Supporting Information).

The intermolecular contacts of the methyl group are all greater than the sum of the van der Waals radii with the exception of a close contact to a carbonyl oxygen atom in n-salt I, and hence small variations in the methyl rotation are not expected to significantly alter the predicted lattice energies. Hence, in all reported minimizations, the rotation of the methyl group was defined via ab initio calculations on the isolated ions, neglecting the effect of the packing forces. However, the experimental structures suggest that other conformational differences could be important. The improper dihedral C4−C3−C2−CH_3 of the experimental molecular conformation of the anion in the racemic structure is 141.5° (referred to [1]-*R*), which is markedly different from the values of 122.0−124.0° found in the other experimental crystal structures and ab initio molecular conformations. This discrepancy may be attributed to experimental inaccuracies, particularly as this structure determination also shows an energetically unfavorable near-eclipsed configuration of the methyl hydrogen atoms.

The repeated crystal structure determinations allow an assessment of the experimental uncertainties and temperature effects. The reduced cell lengths for the low-temperature (150 K) determination of the p-salt (PMACEP0x)[35] contract by

TABLE 2: Reproduction of the p-Salt Crystal Structure[a]

	molecular conformation (anion/cation)		lattice energy			reduced cell parameters[b]				reproduction quality[c]		
	rms[d](Å)	ΔE^e (kJ mol^{-1})	U^f (kJ mol^{-1})	$U^f + \Delta E^e$ (kJ mol^{-1})	density (g cm^{-3})	a (Å)	b (Å)	c (Å)	α (deg)	F	rms	XPRD
p-Salt (*S*)-1-Phenylethylammonium (*R*)-2-Phenylpropanoate **(CSD Reference PMACEP01)** $P2_1$, $Z' = 1$, Room Temperature, $R = 4.49\%$												
experimental[g]					1.108	6.570	11.225	12.257	115.8			
expt[h]	0.000/		−674.92		1.139	6.649	10.986	12.033	115.8	14.10	0.183	0.982
	0.000		(−7.82)		+2.80%	+1.20%	−2.13%	−1.83%	+0.0			
p-Salt (*R*)-1-Phenylethylammonium (*S*)-2-Phenylpropanoate **(CSD Reference PMACEP0x)** $P2_1$, $Z' = 1$, 150 K, $R = 4.07\%$												
experimental[i,j]					1.146	6.539	11.008	12.160	116.0			
expt[h]	0.000/		−675.94		1.135	6.740	10.881	11.997	115.6	22.03	0.190	0.967
	0.000		(−8.20)		−0.96%	+3.07%	−1.15%	−1.3%	−0.4			
in vacuo[j]	**0.221/**	**0.00/**	**−647.86**	**−647.86**	**1.134**	**6.550**	**11.163**	**12.090**	**116.0**	**27.95**	**0.406**	**0.981**
	0.073	**0.00**	**(−25.34)**		**−1.05%**	**+0.17%**	**+1.41%**	**−0.58%**	**+0.0**			
CSD[j]	**0.038/**	**4.49/**	**−650.92**	**−645.21**	**1.115**	**6.746**	**11.075**	**12.104**	**116.7**	**17.06**	**0.176**	**0.968**
	0.058	**1.22**	**(−7.98)**		**−2.71%**	**+3.17%**	**+0.61%**	**−0.46%**	**+0.7**			
$\{\theta_1,\theta_2\}$	0.047/	3.55/	−652.26	−648.71	1.137	6.760	10.907	11.901	115.4	31.91	0.239	0.961
ConOpt	0.073	0.00	(−12.60)		−0.79%	+3.38%	−0.92%	−2.13%	−0.6			
$\{\theta_1,\theta_2,\theta_3,\theta_4\}$	0.047/	3.55/	−652.83	−648.48	1.126	6.720	11.036	12.042	116.4	16.15	0.173	0.969
ConOpt	0.023	0.80	(−6.70)		−1.75%	+2.77%	+0.25%	−0.97%	+0.4			
$\{\theta_1,\theta_2,\omega,\theta_3,\theta_4\}$	0.053/	10.17/	−661.26	−650.29	1.127	6.685	11.108	12.075	116.9	13.90	0.163	0.973
ConOpt	0.023	0.80	(−6.76)		−1.66%	+2.23%	+0.91%	−0.70%	+0.9			

[a] Molecular conformations used in crystal structure prediction are shown in bold. [b] Lattice angles equal to 90° are omitted. [c] Similarity between the experimental and the minimized crystal is established on the basis of the following quantities: the measure of the overall distortion F of the unit cell during the lattice energy minimization defined as a weighted sum of the total rigid-body displacements and translations and unit-cell parameters' change,[92] the coordination sphere root-mean-square discrepancy computed[58] for a 15-ion cluster, the similarity of the simulated powder diffraction pattern between 10° and 50° computed[57] with a 2° width for the triangle function and the unit-cell parameters normalized so as to reproduce the expected unit-cell volumes at room temperature.[93] [d] The optimal positioning of the ab initio ion conformations in the experimental crystal structure is found by rigid-body rotation and translation so as to minimize the rms distance of the non-hydrogen atoms. [e] Conformational optimizations and charge density calculations are performed at the MP2/6-31(d,p) level of theory. [f] Lattice energy (in kJ mol^{-1} asymmetric unit) due to the intermolecular interactions; the value in brackets corresponds to the intermolecular energy reduction during the lattice energy minimization. [g] Reference 38. [h] Hydrogen atom positions adjusted to respect standard neutron values[67] for the bond length N−H. [i] Reference 35. [j] The internal degrees of freedom θ_1, θ_2, ω, θ_3, and θ_4 for the experimental (PMACEP0x), in-vacuo-optimized, and CSD molecular conformations are {−61.87°, 92.69°, 124.61°, 66.56°, −69.85°}, {−49.56°, 72.68°, 130.12°, 73.98°, −61.51°}, and {−64.89°, 94.30°, 130.89°, 59.75°, −61.98°}, respectively.

0.47%, 1.93%, and 0.80% with respect to the room-temperature determination (PMACEP01),[38] resulting in 3.43% higher density (Table 2). Although this anisotropic cell thermal expansion is significant, the molecular conformations are similar with a maximum difference of 1.76° in the rotation of the phenyl group of the anion. However, the two room-temperature determinations of n-salt I (NMACEP[34] and NMACEP02[38]) are characterized by similar cell parameters but markedly different carboxylate O−C−O angles ω (126.6° and 122.1°, respectively), which exemplify the presence of uncertainties in the experimentally determined structures.

3.2.2. Lattice Energy Minimization with the Experimental Molecular Conformations. To assess the accuracy of the intermolecular potential model, we performed lattice energy minimizations with the experimentally determined molecular conformations in which the positions of the hydrogen atoms were corrected to standard neutron X−H bond length values.[67,68] This corrects for the systematic foreshortening of the X−H bond lengths in X-ray diffraction[69] and the artifact that the N−H and methyl C−H bond lengths may shrink due to any librational motions.[70] However, this correction does not allow for the possibility that the N−H hydrogen bond may be elongated in salt structures because of the strong hydrogen bond.[71] We note that the shortest O···H distances of 1.646 and 1.719 Å, observed in the n-salt II and n-salt I polymorphs, respectively, correspond to the longest X-ray N−H bond lengths of 1.055 and 1.024 Å (Table S1 in the Supporting Information).

The results of the minimization of the experimentally known crystals with the experimental ion conformations (expt rows in Tables 2, 3, 4, and 5 for the p-salt, n-salt I, n-salt II, and racemic forms) demonstrate that all known forms are accurately modeled with errors in the reduced lattice lengths smaller than 3.3% with an exception being the racemic compound. This agreement is satisfactory[47,72] because it is comparable to the thermal expansion of organic crystals[73] and suggests that the employed potential model is sufficiently accurate for the modeling of the 1-phenylethylammonium 2-phenylpropanoate crystals. The minimization of the racemic compound with the ab-initio-optimized molecular conformations with the torsion angles θ_1, θ_2, θ_3, and θ_4 and the carboxylate angle ω constrained to their experimental values ($\{\theta_1, \theta_2, \omega, \theta_3, \theta_4\}$ ConOpt row in Table 5) led to significantly lower discrepancies. This suggests that the poor reproduction of the racemic structure with the experimental molecular conformation is probably because of experimental inaccuracies in the molecular geometry, particularly the methyl position, rather than inaccuracies of the intermolecular potential.

Although the overall reproduction of the hydrogen-bonding geometries in the known structures is satisfactory (Table S1 in the Supporting Information), our potential model seems to systematically underestimate the hydrogen-bond lengths $\delta_{N\cdots O}$ by an average 0.07 and 0.10 Å for the enantiomorphous salts (p-salt, n-salt I, and n-salt II) and the less accurately reproduced racemic compound, respectively. This discrepancy cannot be ascribed to thermal expansion effects, because the difference in hydrogen-bond lengths between the low- and room-temperature determinations of the p-salt is modest, suggesting that the shortening of the hydrogen-bond lengths may be due to the use of a rigid-body model with a uniform slightly underestimated value of 1.01 Å for all N−H bond lengths.

TABLE 3: Reproduction of the Crystal Structure of Polymorph I of the n-Salt[a]

	molecular conformation (anion/cation)		lattice energy			reduced cell parameters[b]				reproduction quality[c]		
	rms[d](Å)	ΔE^e (kJ mol^{-1})	U^f (kJ mol^{-1})	$U^f + \Delta E^e$ (kJ mol^{-1})	density (g cm^{-3})	a (Å)	b (Å)	c (Å)	β (deg)	F	rms	XPRD
n-Salt (*R*)-1-Phenylethylammonium (*R*)-2-Phenylpropanoate												
Polymorph I (CSD Reference NMACEP) $P2_12_12_1$, Room Temperature, $R = 7.8\%$, Hydrogen Atom Positions Not Determined												
experimental[g]					1.176	5.800	15.470	17.080	90.0			
expt[h]	0.000/		−661.95		1.150	5.927	15.634	16.772	90.0	15.88	0.152	0.980
	0.000		(−4.06)		−2.21%	+2.19%	+1.06%	−1.80%				
in vacuo	**0.230/**	**0.00/**	**−636.53**	**−636.53**	**1.117**	**6.375**	**15.436**	**16.398**	**90.0**	**196.58**	**0.595**	**0.840**
	0.102	**0.00**	**(−23.40)**		**−5.02%**	**+9.91%**	**−0.22%**	**−3.99%**				
$\{\theta_1,\theta_2\}$	0.045/	3.80/	−651.06	−647.26	1.155	6.108	15.467	16.515	90.0	58.29	0.254	0.927
ConOpt	0.102	0.00	(−10.65)		−1.79%	+5.31%	−0.02%	−3.31%				
$\{\theta_1,\theta_2,\theta_3\}$	0.045/	3.80/	−651.10	−647.22	1.155	6.067	15.447	16.648	90.0	39.65	0.226	0.941
ConOpt	0.066	0.08	(−7.31)		−1.79%	+4.60%	−0.15%	−2.53%				
$\{\theta_1,\theta_2,\omega,\theta_3\}$	0.039/	7.01/	−658.83	−651.74	1.162	6.002	15.471	16.705	90.0	27.46	0.201	0.957
ConOpt	0.066	0.08	(−5.86)		−1.19%	+3.48%	+0.01%	−2.20%				
n-Salt (*R*)-1-Phenylethylammonium (*R*)-2-Phenylpropanoate												
Polymorph I (CSD Reference NMACEP02) $P2_12_12_1$, Room Temperature, $R = 4.27\%$												
experimental[i]					1.179	5.797	15.444	17.073	90.0			
expt[j]	0.000/		−684.42		1.196	5.805	15.466	16.781	90.0	7.15	0.112	0.992
	0.000		(−4.41)		+1.44%	+0.14%	+0.14%	−1.71%				
in vacuo	0.227/	0.00/	**−636.55**	**−636.55**	**1.117**	**6.375**	**15.436**	**16.398**	**90.0**	**183.40**	**0.615**	**0.841**
	0.090	0.00	**(−24.89)**		**−5.26%**	**+9.97%**	**−0.05%**	**−3.95%**				
CSD	0.193/	4.49/	**−632.05**	**−626.34**	**1.125**	**6.109**	**15.300**	**17.139**	**90.0**	**54.23**	**0.383**	**0.940**
	0.080	1.22	**(−19.03)**		**−4.58%**	**+5.38%**	**−0.93%**	**+0.39%**				
$\{\theta_1,\theta_2\}$	0.051/	3.71/	−651.15	−647.44	1.156	6.108	15.469	16.509	90.0	58.52	0.257	0.929
ConOpt	0.090	0.00	(−9.19)		−1.95%	+5.36%	+0.16%	−3.30%				
$\{\theta_1,\theta_2,\theta_3,\theta_4\}$	0.051/	3.71/	−650.80	−646.79	1.158	6.052	15.463	16.636	90.0	37.93	0.211	0.946
ConOpt	0.067	0.30	(−6.22)		−1.78%	+4.40%	+0.12%	−2.56%				
$\{\theta_1,\theta_2,\omega,\theta_3,\theta_4\}$	0.044/	17.39/	−665.79	−648.10	1.170	5.931	15.510	16.747	90.0	16.37	0.167	0.974
ConOpt	0.067	0.30	(−4.19)		−0.76%	+2.31%	+0.43%	−1.91%				

[a−f] Refer to footnotes in Table 2. [g] Reference 34. [h] The protons are placed at the ab-initio-optimized positions from gas-phase calculations by freezing all internal degrees of freedom pertaining to the relative position of the non-hydrogen atoms to their experimental values. The resulting N−H···O angles are found to lie reasonably close to the most probable values as identified by the CSD survey. (See also Table S1 in the Supporting Information.) [i] Reference 38; the internal degrees of freedom θ_1, θ_2, ω, θ_3, and θ_4 for the experimental (NMACEP02) molecular conformation are {71.13°, −73.28°, 122.10°, 69.28°, −56.08°}. [j] Hydrogen atom positions adjusted to respect standard neutron values[67] for the bond length N−H.

TABLE 4: Reproduction of the Crystal Structure of Polymorph II of the n-Salt[a]

	molecular conformation (anion/cation)		lattice energy			reduced cell parameters[b]				reproduction quality[c]		
	rms[d] (Å)	ΔE^e (kJ mol^{-1})	U^f (kJ mol^{-1})	$U^f + \Delta E^e$ (kJ mol^{-1})	density (g cm^{-3})	a (Å)	b (Å)	c (Å)	β (deg)	F	rms	XPRD
n-Salt (*R*)-1-Phenylethylammonium (*R*)-2-Phenylpropanoate												
Polymorph II (CSD Reference NMACEP01) $P2_12_12_1$, Room Temperature, $R = 3.15\%$												
experimental[g]					1.121	5.941	15.469	17.501	90.0			
expt[h]	0.000/		−678.81		1.147	5.944	15.623	16.924	90.0	27.06	0.200	0.979
	0.000		(−4.48)		+2.32%	+0.05%	+1.00%	−3.30%				
in vacuo[i]	**0.327/**	**0.00/**	**−608.49**	**−608.49**	**1.022**	**6.400**	**15.792**	**17.441**	**90.0**	**144.50**	**0.752**	**0.859**
	0.181	**0.00**			**−8.83%**	**+7.73%**	**+2.09%**	**−0.34%**				
			−615.41	**−615.41**	**1.023**	**6.529**	**15.256**	**17.922**	**99.1**	**>500**	**0.753**	**0.859**
			(−53.21)		**−8.74%**	**+9.90%**	**−1.38%**	**+2.41**	**+9.1**			
CSD	**0.169/**	**4.49/**	**−639.44**	**−633.73**	**1.110**	**6.241**	**15.657**	**16.612**	**90.0**	**91.98**	**0.335**	**0.949**
	0.073	**1.22**	**(−15.32)**		**−0.98%**	**+5.05%**	**+1.22%**	**−5.08%**				
$\{\theta_1,\theta_2\}$	0.056/	5.86/	−640.08	−634.22	1.101	6.340	15.661	16.487	90.0	136.87	0.415	0.941
ConOpt	0.181	0.00	(−21.89)		−1.78%	+6.72%	+1.24%	−5.79%				
$\{\theta_1,\theta_2,\theta_3,\theta_4\}$	0.056/	5.86/	−647.20	−639.05	1.103	6.212	15.627	16.825	90.0	63.40	0.287	0.962
ConOpt	0.055	2.29	(−6.81)		−1.61%	+4.56%	+1.02%	−3.86%				
$\{\theta_1,\theta_2,\omega,\theta_3,\theta_4\}$	0.063/	16.71/	−658.98	−639.98	1.110	6.120	15.645	16.958	90.0	39.48	0.248	0.972
ConOpt	0.055	2.29	(−5.88)		−0.98%	+3.01%	+1.14%	−3.10%				

[a−f] Refer to footnotes in Table 2. [g] Reference 38; the internal degrees of freedom θ_1, θ_2, ω, θ_3, and θ_4 for the experimental (NMACEP01) molecular conformation are {76.26°, −87.39°, 123.31°, 56.62°, −70.50°}. [h] Hydrogen atom positions adjusted to respect standard neutron values[67] for the bond length N−H. [i] The minimum was a saddle point (first row); removal of two screw axes led to a $P2_1$, $Z' = 2$ structure (second row).

3.2.3. Lattice Energy Dependence on the Packing-Induced Molecular Distortions. To address the effect of the molecular flexibility on the computed lattice energies and the overall agreement between the minimized and the experimental crystal structures, we have prepared a set of molecular conformations by performing high-level ab initio optimizations of the experimental molecular geometries by freezing various subsets of the soft degrees of freedom to their experimental values, emulating the deformation of the latter from the in vacuo values under the packing forces in the crystal. The results of the rigid-body lattice energy minimizations with the ab-initio-optimized molecular conformations (in vacuo) are shown in Table 2 for the

TABLE 5: Reproduction of the Crystal Structure of the Racemic Form

	molecular conformation (anion/cation)		lattice energy			reduced cell parameters[a]				reproduction quality[b]		
	rms[c] (Å)	ΔE^d (kJ mol^{-1})	U[e] (kJ mol^{-1})	$U^e + \Delta E^d$ (kJ mol^{-1})	density (g cm^{-3})	*a* (Å)	*b* (Å)	*c* (Å)	β (deg)	F	rms	XPRD
Racemic (*R*,*S*)-1-Phenylethylammonium (*R*,*S*)-2-Phenylpropanoate												
(CSD Reference IWIMAC) $P\,2_1/c$, 100 K, $R = 7.18\%$												
experimental[f]					1.093	6.091	15.273	17.875	97.4			
expt[g]	0.000/		−684.35		1.144	6.087	15.517	16.708	93.2	105.66	0.393	0.857
	0.000		(−10.18)		+4.67%	−0.07%	+1.60%	−6.53%	−4.2			
in vacuo	0.304/	0.00/	−628.55	−628.55	1.101	6.454	15.029	17.022	97.4	129.14	0.582	0.950
	0.192	0.00	(−60.27)		+0.73%	+5.96%	−1.60%	−4.77%	+0.0			
$\{\theta_1,\theta_2\}$	0.116/	7.12/	−650.25	−643.13	1.108	6.418	15.399	16.678	99.2	234.98	0.560	0.898
ConOpt	0.192	0.00	(−38.20)		+1.37%	+5.37%	+0.82%	−6.70%	+1.8			
$\{\theta_1,\theta_2,\theta_3,\theta_4\}$	0.116/	7.12/	−650.45	−641.03	1.088	6.285	15.132	17.634	98.9	31.90	0.256	0.952
ConOpt	0.063	2.30	(−11.32)		−0.46%	+3.19%	−0.92%	−1.35%	+1.5			
$\{\theta_1,\theta_2,\omega,\theta_3,\theta_4\}$	0.115/	17.02/	−661.20	−641.88	1.094	6.206	15.198	17.641	98.1	20.57	0.240	0.976
ConOpt	0.063	2.30	(−10.74)		+0.09%	+1.89%	−0.49%	−1.31%	+0.7			

[a−e] Correspond to footnotes [b−f] in Table 2, respectively. [f] Reference 38; the internal degrees of freedom θ_1, θ_2, ω, θ_3, and θ_4 for the experimental (*R*)-1-phenylethylammonium (*R*)-2-phenylpropanoate molecular conformations are {77.16°, −97.42°, 123.73°, 56.05°, −69.21°}. [g] Hydrogen atom positions adjusted to respect standard neutron values[67] for the bond length N−H.

p-salt, Tables 3 and 4 for the n-salt polymorphs, and Table 5 for the racemic form.

In all cases, apart from the racemic form, the minimizations with the in vacuo conformations lead to worse reproductions of the crystal structures in comparison to the minimizations with the experimental molecular conformations (expt). In the case of the low-temperature determination of the p-salt (PMACEP0x), the in vacuo and experimental molecular conformation of the anion and cation differ by a root-mean-square (rms) displacement of 0.221 and 0.073 Å, respectively, with the largest packing-induced distortion being a 20° increase in the carboxylate group rotation θ_2. Despite these conformational changes, the expt and in vacuo lattice energy minimizations lead to similar overall discrepancy values ($F = 22.03$ and 27.95, respectively) and simulated XRPD changes, although the minimum obtained with the in vacuo conformations is characterized by a significantly higher rms discrepancy of the 15-molecule coordination sphere (0.406 Å compared with 0.190 Å of expt anion expt cation). Hence, the ability to model the p-salt by rigid-ion lattice energy minimization is satisfactory even if the packing-induced distortions are neglected.

In contrast, the reproductions of the n-salt polymorphs and the racemic form appear to be significantly more sensitive to the packing-induced molecular conformations (Tables 3−5). In the case of the NMACEP02 determination of n-salt I, there are large percentage errors in the modeling of the reduced lattice length parameters with the in vacuo ion conformations, although the rms differences between the latter and experimental ion geometries are similar to those for the p-salt. In the case of n-salt II (NMACEP01), the minimization leads to a saddle point; the removal of the screw axes along the **a** and **b** directions followed by a line search in the direction of decreasing energy and resumption of the minimization at the lowest point produced a $P2_1$, $Z' = 2$ structure that was 6.9 kJ mol^{-1} lower in energy.

The computed intermolecular energies are all very sensitive to even small conformational changes. The intermolecular lattice energy is consistently stabilized as more internal coordinates are constrained to their experimental values (Tables 2−5). This result suggests that the deformation of the ion geometries from their in vacuo geometries improves the intermolecular interactions in the experimental crystal structures. This more than compensates for the increased intramolecular energy penalty due to the packing-induced distortions of the ion geometries. Constraining the torsion angles θ_1 and θ_2 of the anion to their experimental values reduces the lattice energy by 4.40, 14.60, and 24.67 kJ mol^{-1} in the case of the p-salt (PMACEP0x), n-salt I (NMACEP02), and n-salt II, respectively, while the intramolecular energy increases by 3.55, 3.71, and 5.86 kJ mol^{-1}. The intermolecular energy is significantly less dependent on the cation geometry as shown by the modest effect on the lattice energies when the torsion angles θ_3 and θ_4 are additionally constrained to their experimental values. The intermolecular energies for the p-salt (PMACEP0x), n-salt I (NMACEP02), and racemic compound are practically unaffected by the slight variations in the rotation of the phenyl and ammonium groups, while the intermolecular energy of the n-salt II form is reduced by 7.12 kJ mol^{-1}, presumably because this form is characterized by the shortest hydrogen-bond length $\delta_{N\cdots O}$ (2.693 Å, Table S1 in the Supporting Information). Once more, the more favorable intermolecular interactions compensate for the modest increase of 2.29 kJ mol^{-1} in intramolecular energy.

Finally, the intermolecular lattice energies seem to be a strong function of the carboxylate angle ω. The ab initio optimizations at the MP2/6-31G(d,p) level of theory overestimate this angle by approximately 6°, which is responsible for an average increase in intermolecular energy of 11 kJ mol^{-1}. This result suggests that the 7 kJ mol^{-1} intermolecular energy difference between the $\{\theta_1,\theta_2,\theta_3,\theta_4,\omega\}$-constrained ab initio conformations for the two determinations of the n-salt I (NMACEP and NMACEP02) is mainly because of the 4.5° discrepancy in the carboxylate angle. Although the ammonium hydrogens are involved in strong hydrogen bonds, the rotation of the ammonium group θ_4 by 5° has only a minor effect on the intermolecular and total lattice energy as shown by the comparison of the $\{\theta_1,\theta_2,\theta_3\}$-constrained NMACEP and $\{\theta_1,\theta_2,\theta_3,\theta_4\}$-constrained NMACEP01 minimizations. Concluding, the significant sensitivity of the lattice energy to the fine details of the molecular conformations, in conjunction with the presence of experimental uncertainties, limits the accuracy of the predicted relative stability to a few kilojoules per mole.

3.2.4. Experimental and Calculated Relative Stabilities of the Known Crystal Structures. Differential scanning calorimetry measurements[37] revealed that n-salt I undergoes an endothermic transformation to n-salt II (at 104.7 °C) prior to melting (148.8 °C). The endothermic transformation in conjunction with the lower density of the n-salt II polymorph at room temperatures (the density of NMACEP01 is 1.12 g cm^{-3} compared to 1.18 g cm^{-3} for NMACEP02) suggests an enantiotropic relation with

a transition point below the transformation temperature. This implies that the lattice energy of n-salt I should be lower than that of n-salt II, although exceptions to the heat of transition and density rules are known.[74,75] The p-salt has lower solubility[36] at ambient temperatures than n-salt I, and thus it is more stable. Moreover, the solubility ratio, and hence free energy difference, between the two salts increases with increasing temperature.[36] From the available solubility measurements, we can estimate that the free energy differences $G_{\text{p-salt}} - G_{\text{n-salt I}}$ at 10 and 30 °C are −1.35 and −1.87 kJ mol^{-1}, respectively. Solution calorimetry measurements at 25 °C reveal that the enthalpy of the p-salt is approximately 3.9 kJ mol^{-1} higher than that of the n-salt I form,[76] implying that the lattice energy of n-salt I should be lower (more negative) than that of the p-salt. Interpolation of the free energy difference at 25 °C and consideration of the enthalpy differences leads to the conclusion that the entropy of the p-salt is 18.9 J K^{-1} mol^{-1} higher than the entropy of n-salt I, which is consistent with the significantly lower density of the p-salt at room temperature (1.108 g cm^{-3} compared to 1.179 g cm^{-3}, see Tables 2 and 3). The racemic salt is probably the least stable form as annealing experiments in the temperature range 50−70 °C revealed an irreversible first-order transformation of the sample into the stable [1]-*S*−[2]-*R*, [1]-*R*−[2]-*S* conglomerate. Thus, the experimental evidence suggests the following stability relations at room temperature, p-salt ≈ n-salt I > n-salt II > racemic, where the stabilities of the p-salt and n-salt I are close, as discussed further in section 4. We can speculate that the same stability order applies at 0 K, although the range of experimental data does not suffice to allow this extrapolation to be made with confidence.

Despite the significant sensitivity of the intermolecular energy to minor conformational changes, the total lattice energy $\Delta E + U$ appears to converge to a stable value when more internal degrees of freedom are gradually constrained to their experimental values. If we focus on the results with the $\{\theta_1,\theta_2,\theta_3,\theta_4\}$-constrained conformations, then the most accurate determination of the n-salt I form (NMACEP02) is approximately 2 kJ mol^{-1} less stable than the p-salt (PMACEP0x) and approximately 8 kJ mol^{-1} more stable than the second polymorph n-salt II (NMACEP01). The racemic form (IWIMAC) appears to be 2 kJ mol^{-1} more stable than the n-salt II form, although the accuracy of its predicted relative stability is very dependent on possible errors in the experimental determination of the molecular conformation of the anion. The predicted stability order, p-salt ≈ n-salt I > n-salt II ≈ racemic, is not affected when the carboxylate angle is also constrained to its experimental value for the most recent determination of the each form. (In contrast to the results from NMACEP02, the NMACEP determination of the n-salt I form becomes 1.5 kJ mol^{-1} more stable than the p-salt, showing that the experimental uncertainty in the molecular geometries is a limitation in estimating the relative lattice energies.) Thus, the predicted relative stability of the known forms is in reasonable agreement with the experimental evidence.

3.3. Statistical Analysis of the CSD to Determine Probable Ion-Pair Geometries. The ISOSTAR[77] plot of the probability density for the position of carboxylate oxygen atoms in the vicinity of charged amino groups derived from 1224 entries in the Cambridge Structural Database[30] and Protein Data Bank[78,79] (shown in the Supporting Information) shows that carboxylate oxygen acceptors are in relatively confined regions of space around the ammonium group, whose positions are consistent with the classical N−H···O hydrogen-bond geometry. This implies that it is possible to determine relatively narrow regions for at least some of the lengths, angles, and torsions defining the ion-cluster geometry on statistical grounds and restrict the search to geometries that have been observed in experimentally determined crystal structures.

The probability densities for all six variables needed to define the ion-cluster geometry are shown in Figure 7 (which also includes the position of the ammonium hydrogen atoms) and were derived from a set of 881 unique crystal structures with 2794 $RCCNH_3^+$ and $RCCOO^-$ close contacts. The distribution for the $\delta_{N\cdots O}$ distances shows the sharpness expected for strong hydrogen bonds[80] and has an average of $\mu_{\delta_{N\cdots O}} = 2.82$ Å and standard deviation $\sigma_{\delta_{N\cdots O}} = 0.084$ Å. These values compare well with the results of an earlier statistical study of 1357 NH···O bonds, including nonionic interactions ($\mu_{\delta_{N\cdots O}} = 2.89$ Å, $\sigma_{\delta_{N\cdots O}} = 0.112$ Å),[81] although our slightly shorter average $\delta_{N\cdots O}$ distance can be attributed to the strength of the hydrogen bonds in salts and the smaller deviation to a restricted search of similar natures and environments of the donor and acceptor groups. The distribution for the hydrogen-bond angles $\omega_{NH\cdots O}$ exhibits two peaks at 55° and 170°. The smaller of the peaks is due to the hydrogen atom involved in the hydrogen bond. (The position of the other peak is a direct consequence of the linearity of the NH···O hydrogen bond and the tetrahedral geometry of the ammonium group, and it is due to the two hydrogen atoms that are not involved in the hydrogen bond.) The distribution of the $\omega_{CN\cdots O}$ angle (Figure 7c) exhibits a peak at around 110°, which is approximately the tetrahedral angle in the ammonium group and also reflects the linearity of the NH···O hydrogen bond. The last degree of freedom for the determination of the position of the hydrogen-bonded oxygen atom with respect to the ammonium cation, the torsion angle $\phi_{CCN\cdots O}$, has a distribution (Figure 7d) that exhibits three peaks. Their positions can be explained by the linearity of the NH···O hydrogen bond and the tendency of the substituents of the four-coordinate N and C atoms to avoid the energetically unfavorable eclipse conformation. Of the other three degrees of freedom required to define the position of the anion with respect to the cation, only the distribution of the angle $\omega_{N\cdots OC}$ (Figure 7e) is restricted to a relatively confined region. Its peak at about 120° is consistent with the position of the lone pairs of the oxygen atom involved in the hydrogen bond.[82] The probability distributions (Figures 7f and 7g) for the torsion angles $\phi_{CN\cdots OC}$ and $\phi_{N\cdots OCC}$, which correspond to the rotation of the anion around the hydrogen bond axis and the rotation of the anion around the C═O carboxylate bond, respectively, are significant for the entire range of angles, showing that the search should sample the entire space. However, the broad peaks of the $\phi_{N\cdots OCC}$ distribution at ±180° and 0° suggest that there is a weak preference for the atoms N···OCC to lie on the same plane.

Overall, the derived probability density distributions exhibit peaks at chemically intuitive angles, providing at the same time information on the variance of the sampled variables based on a sufficiently large set of distinct experimentally resolved crystal structures. If we eliminate the areas with probability densities smaller than 0.1 times its maximum value, then the following regions should be accessible in the crystal structure prediction search: $\delta_{N\cdots O} \in [2.69\text{ Å}, 3.01\text{ Å}]$, $\omega_{CN\cdots O} \in [90°, 130°]$, $\phi_{CCN\cdots O} \in [-180°, -154°] \times [-88°, -37°] \times [29°, 88°] \times [154°, 180°]$, $\omega_{N\cdots OC} \in [97°, 156°]$, $\phi_{CN\cdots OC} \in [-180°, 180°]$, and $\phi_{N\cdots OCC} \in [-180°, 180°]$. Because the relative position and orientation of the two ions are relaxed in the lattice energy minimization, we only need to ensure that the initial ion-pair geometries are defined so that all local minima are accessible. Given the sharpness of their distributions, only the most probable

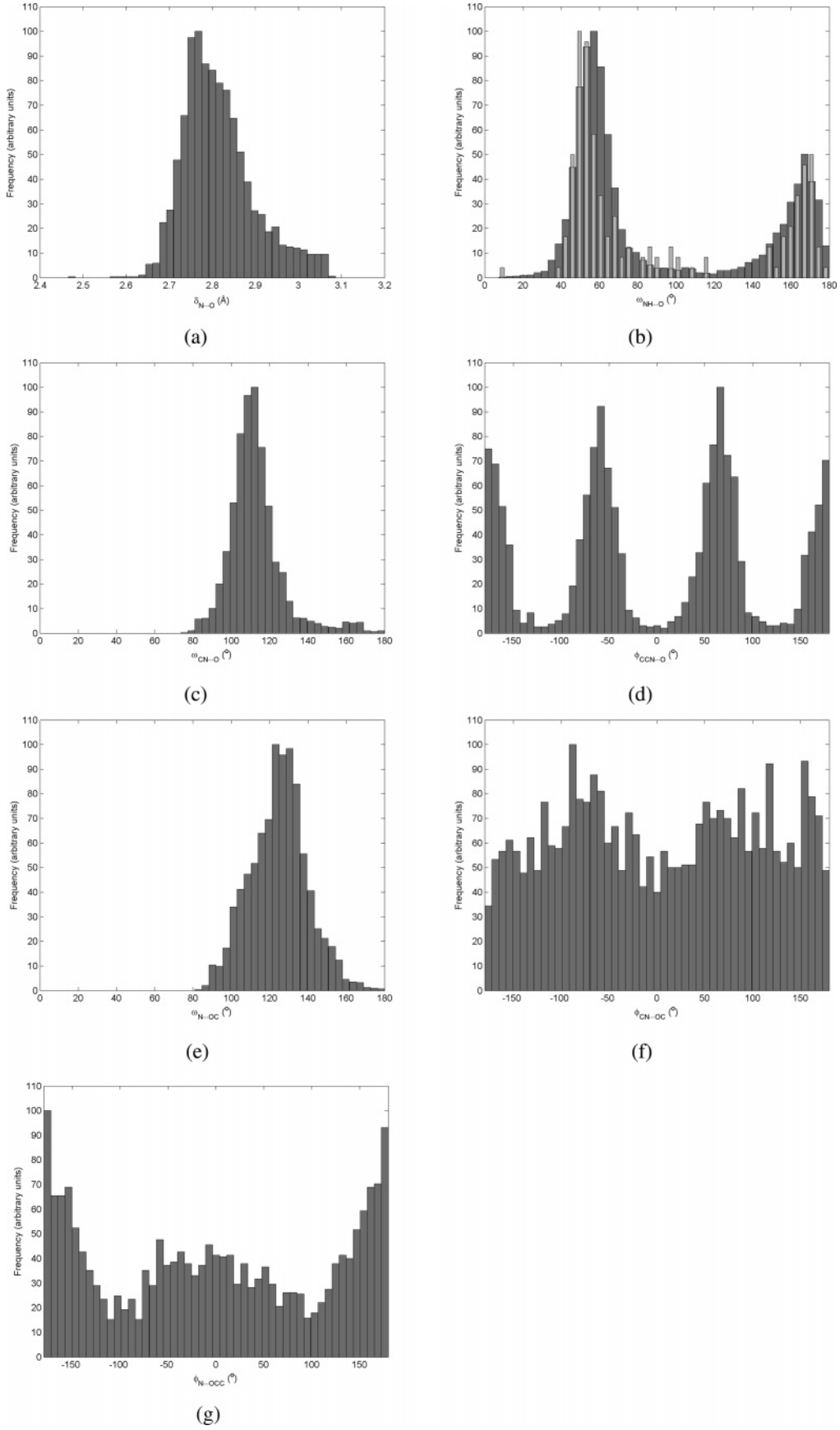

Figure 7. Histograms of the $RCNH_3^+\cdots{}^-OOCCR$ close contacts. (a) N···O hydrogen-bond length, (b) NH···O hydrogen-bond angle, light gray is the result of the analysis of 55 close contacts in the subset of 20 crystal structures determined by neutron scattering, (c) CN···O angle, (d) CCN···O torsion, (e) N···OC angle, (f) CN···OC torsion, (g) N···OCC torsion. Each probability distribution has been normalized to give a maximum value of 100, without corrections for any geometric factors. (For example, the distribution for the $\omega_{NH\cdots O}$ angles (b) is uncorrected by the geometric factor that the number of possible configurations with $y - \delta y < \omega_{NH\cdots O} < y + \delta y$ proportional to sin y, and hence it exhibits a maximum at near-linear hydorgen-bond geometries.[81,95])

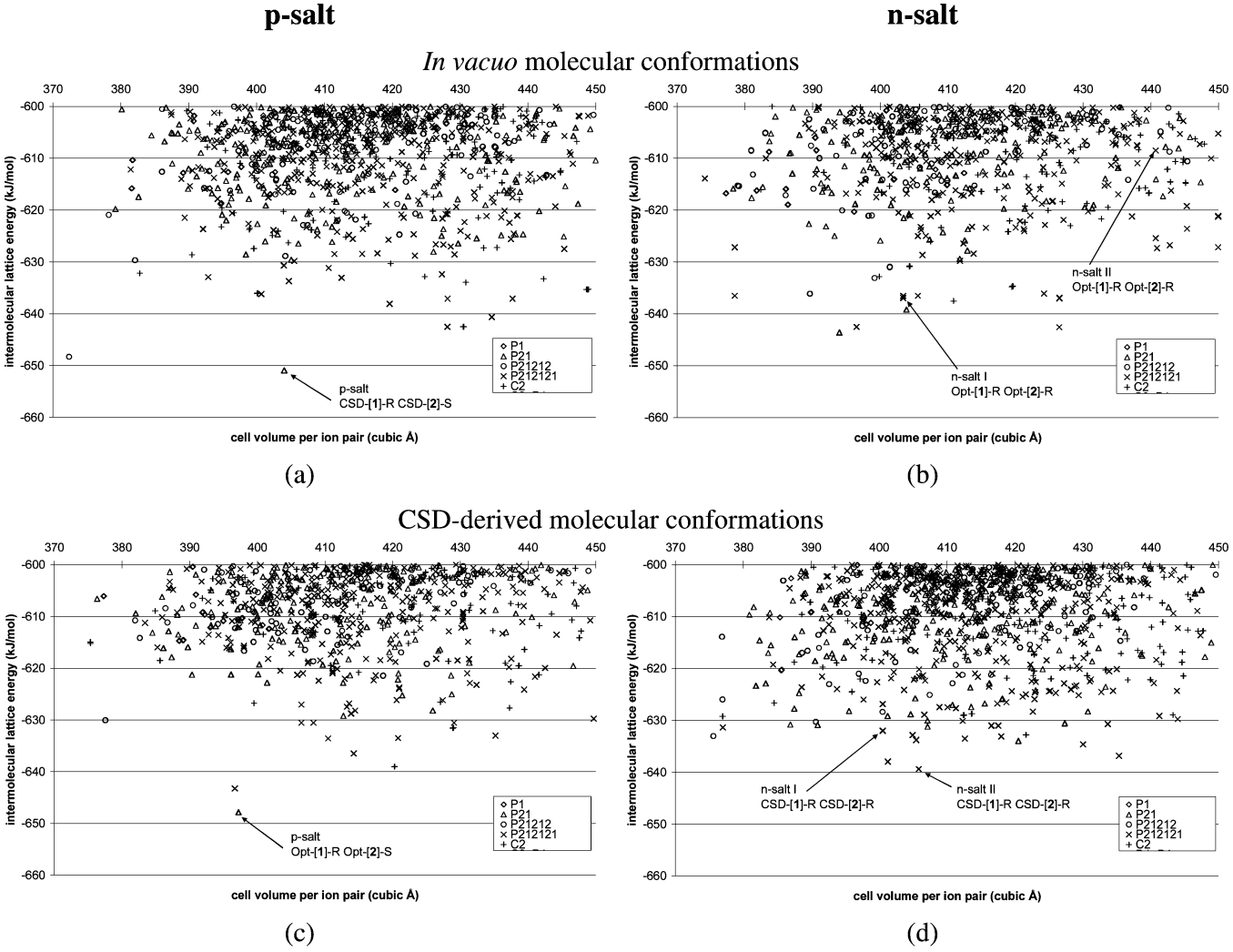

Figure 8. Intermolecular lattice energies of the low-energy crystal structures found in the searches for the p-salt (left) and n-salt (right) diastereomeric pairs of (*R*)-1-phenylethylammonium (*R*/*S*)-2-phenylpropanoate, using the in vacuo geometries (top) and CSD-derived (bottom) ions. The minima corresponding to the known forms (Table 6) are indicated. To compare total lattice energies for the two sets of conformations, the intramolecular energy penalty for the CSD molecular conformations, estimated at 5.71 kJ mol^{-1}, should be added to the energies shown in the bottom graphs.

values 2.82 Å, 110°, and 120° for the variables $\delta_{N1\cdots O2}$, $\omega_{C7N1\cdots O2}$, and $\omega_{N1\cdots O2C4}$ (Figure 2), respectively, were used to define the initial structures of the ion pairs used in the MOLPAK search. All three donors of the ammonium group were explicitly considered by using the values $\phi_{C6C7N1\cdots O2} = -180°$, $-60°$, and $+60°$. The last two variables $\phi_{C7N1\cdots O2C4}$ and $\phi_{N1\cdots O2C4C3}$ that have the wider probable regions were sampled over the whole region $-180°$ to 180° in 60° intervals, following preliminary tests in which it was established that the experimental structure of the p-salt was found in searches starting from ion-pair clusters in which these torsion angles differed by up to 60°.

The probability distributions only take into account the search moiety (Figure 3), and hence it is possible to generate clusters of probable geometry that are energetically unfavorable due to steric repulsion of the 1-phenylethylammonium 2-phenylpropanoate phenyl and methyl groups. Approximately one-fifth of the 108 ion-pair geometries were discarded because they generated a contact that was significantly smaller than the sum of the van der Waals radii (i.e., less than 2.2 Å for non-hydrogen contacts and 1.2 Å for contacts involving hydrogen). Moreover, 40−50 candidate ion clusters were rejected because preliminary tests showed that the substituents' positions for the specific ion conformations and chirality would result in unused hydrogen-bond donors and acceptors in the crystal. The remaining 20−30 ion-cluster geometries were used as molecular probes for the generation of candidate crystals with MOLPAK.

3.4. Crystal Structure Prediction. Crystal structure prediction studies were performed for both the p-salt ([1]-*R*, [2]-*S*) and the n-salt ([1]-*R*, [2]-*R*) with both the in vacuo ab-initio-optimized molecular conformations and the torsion angles θ_1, θ_2, and θ_3 constrained to the average values observed in the CSD as derived in section 3.1. The distributions of low-energy structures found in these four crystal structure prediction studies are shown in Figure 8.

In the case of the p-salt, the global minimum corresponds to the only experimentally determined form with both sets of molecular conformations (see Table 2 for quality of reproduction). In the majority of the stable structures, the ammonium group is hydrogen-bonded to three oxygen atoms belonging to different carboxylate groups forming R_4^3 (10) rings that are arranged in ladders similar to the ones in the experimentally determined enantiomorphous crystals.[38] Moreover, in the search with the CSD molecular conformations, 10 out of the 20 most stable hypothetical structures show significant similarities to the known p-salt structure, having superimposable hydrogen-bonded ladders, with identical orientation of the phenyl rings of the hydrogen-bonded ions relative to the ladder, but differing in

TABLE 6: Most Stable Unique Crystal Structures for the p-Salt (First 20 Structures) and n-Salt (Last 20 Structures) with the CSD Molecular Conformations[a]

					reduced cell parameters					
number	name of structure[b]	space group	lattice energy (kJ mol^{-1})	volume per asymmetric unit (Å^3)	*a* (Å)	*b* (Å)	*c* (Å)	α (deg)	*β* (deg)	*γ* (deg)
			p-Salt, (*R*)-1-Phenylethylammonium (*S*)-2-Phenylpropanoate							
1	**C12af5**	***P*2$_1$**	**−650.956**	**404.09**	**6.745**	**11.075**	**12.104**	**116.65**	**90.00**	**90.00**
2	D25ba72	*P*2$_1$2$_1$2	−648.323	372.38	5.539	15.301	17.573	90.00	90.00	90.00
3[c]	C7aq87	*P*2$_1$2$_1$2$_1$	−642.596	428.13	6.693	10.998	23.262	90.00	90.00	90.00
4[c]	D36db27	*C*2	−642.544	430.53	6.734	12.020	21.485	98.03	90.00	90.00
5[c]	C12aq57	*P*2$_1$2$_1$2$_1$	−640.676	434.67	6.500	14.513	18.431	90.00	90.00	90.00
6	C25aq25	*P*2$_1$2$_1$2$_1$	−638.131	419.62	6.554	12.609	20.311	90.00	90.00	90.00
7[c]	D15aq21	*P*2$_1$2$_1$2$_1$	−637.129	437.73	6.701	11.900	21.957	90.00	90.00	90.00
8	D25aq83	*P*2$_1$2$_1$2$_1$	−636.233	400.71	6.655	11.335	21.249	90.00	90.00	90.00
9	D19db36	*C*2	−636.112	400.09	6.639	11.351	21.703	101.88	90.00	90.00
10[c]	C13db14	*C*2	−635.344	448.82	6.757	10.933	24.460	96.55	90.00	90.00
11[c]	D15db68	*C*2	−633.969	430.81	6.676	11.639	22.693	102.25	90.00	90.00
12	D7az94	*P*2$_1$2$_1$2$_1$	−633.741	404.79	6.664	9.372	25.926	90.00	90.00	90.00
13[c]	D14db58	*C*2	−633.293	442.30	6.752	12.145	21.652	94.82	90.00	90.00
14	D13aq55	*P*2$_1$2$_1$2$_1$	−633.104	412.56	6.633	12.109	20.545	90.00	90.00	90.00
15	E36az96	*P*2$_1$2$_1$2$_1$	−632.942	392.89	5.803	15.229	17.781	90.00	90.00	90.00
16[c]	D15db21	*C*2	−632.888	424.78	6.625	12.879	20.305	101.27	90.00	90.00
17[c]	C7az118	*P*2$_1$2$_1$2$_1$	−632.399	427.32	6.668	13.037	19.663	90.00	90.00	90.00
18	C30db9	*C*2	−632.199	382.80	5.476	15.375	19.171	108.46	90.00	90.00
19[c]	C12db89	*C*2	−631.846	464.48	6.747	16.519	16.918	99.80	90.00	90.00
20	D13aq105	*P*2$_1$2$_1$2$_1$	−631.171	410.64	6.499	14.794	17.084	90.00	90.00	90.00
			n-Salt, (*R*)-1-Phenylethylammonium (*R*)-2-Phenylpropanoate							
1[d]	**C26aq118**	***P*2$_1$2$_1$2$_1$**	**−639.437**	**405.83**	**6.241**	**15.657**	**16.613**	**90.00**	**90.00**	**90.00**
2	C26az18	*P*2$_1$2$_1$2$_1$	−638.008	401.29	6.613	11.097	21.873	90.00	90.00	90.00
3[d]	D32az117	*P*2$_1$2$_1$2$_1$	−636.837	435.33	6.409	14.654	18.540	90.00	90.00	90.00
4[d]	C26az103	*P*2$_1$2$_1$2$_1$	−634.66	430.05	6.625	11.969	21.695	90.00	90.00	90.00
5[d]	C26af2	*P*2$_1$	−634.016	420.51	6.556	11.235	11.485	96.21	90.00	90.00
6	D12aq12	*P*2$_1$2$_1$2$_1$	−633.82	405.46	6.735	12.339	19.518	90.00	90.00	90.00
7	D13aq33	*P*2$_1$2$_1$2$_1$	−633.545	412.66	6.764	15.543	15.701	90.00	90.00	90.00
8	D25aq30	*P*2$_1$2$_1$2$_1$	−633.14	417.99	7.128	14.077	16.662	90.00	90.00	90.00
9	D5ap42	*P*2$_1$2$_1$2	−633.085	375.58	5.412	15.770	17.600	90.00	90.00	90.00
10	C24aq117	*P*2$_1$2$_1$2$_1$	−632.869	404.91	6.748	9.178	26.151	90.00	90.00	90.00
11[d]	D7db85	*C*2	−632.82	421.62	6.465	11.591	23.004	101.92	90.00	90.00
12[e]	**C24az49**	***P*2$_1$2$_1$2$_1$**	**−632.059**	**400.52**	**6.110**	**15.300**	**17.139**	**90.00**	**90.00**	**90.00**
13	D5az21	*P*2$_1$2$_1$2$_1$	−631.41	376.98	5.270	9.311	30.734	90.00	90.00	90.00
14	C17af21	*P*2$_1$	−631.21	407.15	6.567	8.793	14.297	99.48	90.00	90.00
15	C24az77	*P*2$_1$2$_1$2$_1$	−631.069	416.52	6.751	14.892	16.572	90.00	90.00	90.00
16	C17az57	*P*2$_1$2$_1$2$_1$	−631.06	417.54	6.752	13.086	18.903	90.00	90.00	90.00
17	D36af97	*P*2$_1$	−630.911	390.95	5.253	9.503	15.819	90.00	98.04	90.00
18	E1af83	*P*2$_1$	−630.84	386.93	5.27	9.319	15.878	90.00	97.03	90.00
19[e]	C12az92	*P*2$_1$2$_1$2$_1$	−630.742	433.69	6.517	15.877	16.765	90.00	90.00	90.00
20[d]	D8af86	*P*2$_1$	−630.613	427.32	6.532	11.531	11.813	106.14	90.00	90.00

[a] The rows in bold correspond to the known diastereomeric salt structures: p-salt (global minimum), n-salt II (global minimum), n-salt I (minimum 12). [b] Name of ion-pair cluster (C, D, and E correspond to $\phi_{CCN\cdots O}$ equal to 180 °, 60°, and −60°, respectively, according to which hydrogen atom was hydrogen-bonded in the MOLPAK ion-pair cluster; for each of these categories, we generate 36 cluster geometries by considering the whole range of $\phi_{CN\cdots OC}$ and $\phi_{N\cdots OCC}$ values in increments of 60°) followed by the MOLPAK name for the candidate structure. [c] Crystal structures whose 15-molecule coordination spheres resemble the one in the global minimum (corresponding to the known p-salt form) with at least 9 molecules matching. [d] The global minimum (corresponds to n-salt II) and third minimum are similar with 0.73 Å rms difference in the 15-molecule coordination sphere; the global minimum and minima 4, 5, 11, and 20 have 10 out of the 15 molecules of the coordination sphere matching. [e] Minimum 12 (corresponds to n-salt I) and minimum 19 have 8 molecules of a 15-molecule coordination sphere matching.

the way that the ladders pack. (For these hypothetical structures, 9−11 molecules of the 15-molecule coordination sphere match the p-salt structure within a 20% atom−atom distance tolerance.[58]) Many of the other low-energy hypothetical structures have different orientations of the phenyl groups around the hydrogen-bonded R_4^3 (10) ladders. There are only three structures that do not exhibit the R_4^3 (10) ladder motif with the ammonium group hydrogen-bonded to four oxygen atoms belonging to three (minimum 15) or four carboxylate groups (minima 2 and 18). Thus, the searches have not only identified the known structure as the global minimum but also shown a strong preference for the ladder motif.

The hypothetical polymorphic landscape of the n-salt is more complex, as the search with the CSD molecular conformations produced as many (20) distinct structures within 9 kJ mol^{-1} of the global minimum as were found within 20 kJ mol^{-1} for the p-salt (Table 6 and Figure 8). Of the 20 most stable unique structures predicted as energetically feasible polymorphs in the search with the CSD molecular conformations, only one (minimum 3) had a similar 15-molecule coordination sphere geometry to the global minimum, which corresponded to the n-salt II form (0.73 Å rms error), and four more (minima 4, 5, 11, and 20) were characterized by superimposable hydrogen-bonded ladders (with similar orientation of the phenyl rings) packed in different ways. The minimum corresponding to n-salt I (minimum 12, 7.4 kJ mol^{-1} above the global minimum; see Table 3 for quality of reproduction) exhibits the same hydrogen-bonded ladder geometry as one other structure (minimum 19), although once more the ladders are packed in different ways. The search for the n-salt produces many more distinct hydrogen-

bonding patterns than the one for the p-salt. These include rippled sheets comprising R_6^5 (16) rings (minima 13, 17, and 18), a greater variety in the orientation of the phenyl ring with respect to R_4^3 (10) ladders (minima 15, 2, 7, 16, 8, and 14), structures with the ammonium group bonded to four oxygen atoms (minima 6 and 10), and even more complicated patterns forming channels consisting of R_6^5 (16) and R_4^4 (12) rings (minimum 9). The greater complexity of the energy landscape for the n-salt, with more energetically competitive and distinctive packing arrangements, is consistent with its observed polymorphism.

Although the search for stable n-salt structures with the CSD-derived molecular conformations identified both known forms, the stability order is reversed relative to the calculations with the experimental ion geometries (Tables 3 and 4). This significant sensitivity to the differences in the molecular conformation between our search rigid model and the experimentally determined structures is also seen in the search with the in vacuo conformations in which the n-salt I structure was found seventh, 7.2 kJ mol^{-1} above the global minimum, while the minimum closest matching the n-salt II form was 35 kJ mol^{-1} higher. Thus, the consideration of only the in vacuo ion conformations would not have generated one of the known polymorphs as thermodynamically plausible.

As a further investigation of the sensitivity of the lattice energy surface with respect to the molecular conformation, we performed crystal structure prediction runs with the MP2/6-31G-(d,p) ab-initio-optimized conformations with the rotation of the phenyl and carboxylate groups of the anion fixed to the experimental values of each of the known enantiomorphous salt forms. The search for stable p-salt structures, with the torsion angles θ_1 and θ_2 fixed to the only experimentally determined form, produced the latter at the global minimum (intermolecular lattice energy -652.26 kJ mol^{-1}) that was 7.46 kJ mol^{-1} more stable than the second minimum; i.e., the energy difference was increased with respect to the searches with both CSD and ab-initio-optimized conformations. The search with the set of torsions θ_1 and θ_2 constrained to the n-salt I values produced two similar stable crystals clearly separated by more than 10 kJ mol^{-1} from the rest of the structures, with the global minimum corresponding to the thermodynamically more stable n-salt I. In the search with the θ_1 and θ_2 torsions constrained to the n-salt II values, the global minimum corresponded to the known n-salt I (reproduced with 0.28 Å rms error in the 15-molecule coordination sphere), while the second minimum was 6 kJ mol^{-1} less stable and corresponded to the metastable polymorph n-salt II. Thus, the ranking of the hypothetical n-salt structures is significantly more sensitive to the molecular conformations (mainly the rotation of the phenyl and carboxylate groups of the anion) than the ranking of the p-salt ones, in accordance with the greater sensitivity of the quality of the reproduction and lattice energies to conformational changes during the minimization of the known forms.

Finally, the search with the MP2/6-31G(d,p)-optimized geometry for the cation and the second conformational minimum for the anion ($\theta_1 = -117.68°$, $\theta_2 = 105.62°$) for stable p-salt crystals did not produce any low-energy crystals as the global minimum (intermolecular lattice energy -636.57 kJ mol^{-1}) had 11.87 kJ mol^{-1} higher total energy than the global minimum in the search with the CSD molecular conformations. Thus, this secondary conformational minimum of the anion is worse than the global minimum in producing good crystal packings, in accord with the CSD conformational analysis (Figure 6c).

4. Discussion

The success of the simple search strategy in finding the three known crystal structures of a diastereomeric salt pair, along with a range of other plausible structures, shows that the novel approach of using the range of ion-pair cluster geometries indicated by an analysis of the known crystal structures in the CSD is an effective and practical means of addressing the challenge of the increased dimensionality of crystal structure prediction for salts. Crystal structure prediction of diastereomeric salts is a mathematically challenging problem due to the presence of two molecular fragments in the asymmetric unit, which is compounded by the molecular flexibility around the chiral centers. The proposed methodology establishes an efficient way to generate candidate structures based on a statistical analysis of a large number of experimentally determined crystals, which ensures the most efficient exploration of phase space for a given number of local minimizations and set of molecular conformations. Obviously, the relatively limited number of considered clusters does not ensure a thorough sampling of the computed probability distributions, and hence some minima may have been missed. Since no new stable minima were identified during the last few thousands of local minimizations for all sets of molecular conformations considered, our choices constitute an acceptable compromise between computational cost and thoroughness of the search method. Although more stable crystals may be found if additional, less probable, chiral space groups[83] and/or asymmetric units with more than one pair of ions are considered, the associated computational cost is prohibitive, and the search for such minima remained out of the scope of the present study.

The less expected challenge of crystal structure prediction for diastereomeric salts revealed by this study is that the results of the search for the p- and n-salts are so different. The known structure of the p-salt is readily predicted as the most stable for quite a wide range of conformations of the flexible ions. It is clear that the ladder motif is a thermodynamically favored ion spatial arrangement and the known p-salt form corresponds to its most stable packing. In contrast, the predictions for the n-salt generate a wide range of packing motifs, whose relative stability is extremely sensitive to fine details of the molecular conformation. We may speculate that the greater variety of packing motifs for the n-salt relative to the p-salt is consistent with the much greater difficulty in growing single crystals suitable for X-ray diffraction of either of the n-salt polymorphs. (The recently published single-crystal data[38] came 3 years after the new forms were identified from powder,[37] and recent attempts to grow single crystals consistently produced thin needles.[35])

If we examine the known crystal structures (Tables 2−5), then it is clear that the relative energies of the p-salt and the stable form of the n-salt are very sensitive to the molecular conformation and probably very close, which is consistent with the enthalpy difference of a few kilojoules per mole from solution calorimetry measurements. Predicting the resolution efficiency when the energy differences are so small is clearly a major challenge to evaluating both the p- and the n-salt energies accurately. More generally, a solubility ratio of 2:1 at room temperature, which is probably sufficient for a successful diastereomeric resolution, corresponds to a free energy difference of only 3.4 kJ mol^{-1}, which is comparable to the predictive accuracy of current computational models. In this case, the n-salt's conformational flexibility is so important in determining the relative energies of the known and hypothetical crystal structures that not only do the intramolecular energy penalty and conformers have to be calculated by a high-quality ab initio

method, but it is also not feasible to consider the desired range of conformations over a particularly fine grid for the soft degrees of freedom. This contrasts with the ability to predict the known forms of the p-salt form and the polymorphs of piracetam[84] and 1-hydroxy-7-azabenzotriazole[85] with a limited set of rigid molecular conformations.

The minimizations with the ab-initio-optimized conformations with the soft degrees of freedom frozen to their experimental values (Tables 2−5) demonstrate that the deformation of the in vacuo molecular geometries in the dense crystalline environment facilitates significantly more favorable intermolecular interactions. This is primarily due to the improved electrostatic energy; for example, for the p-salt (PMACEP0x), the electrostatic energy with the in vacuo molecular conformations is −588.65 kJ mol^{-1}, which is reduced consistently when more internal degrees of freedom are constrained to the experimental values until it becomes equal to −622.8 kJ mol^{-1} for the experimental conformations. The repulsion−dispersion energy only increases from −59.2 to −53.1 kJ mol^{-1}. However, this stabilization does not appear to be due to the arrangement of the ions of the carboxylate and ammonium groups. If we model the ions by placing just a +1 charge on nitrogen, $-^1/_2$ on oxygen, and no charge on all other atoms, then the electrostatic intermolecular lattice energies are −630.5 and −641.3 kJ mol^{-1} with the optimized and experimental molecular conformations, respectively. Thus, the change in relative positions of the hydrogen-bond donor and acceptors accounts for only one-third of the reduction in the total electrostatic contribution. Hence, the majority of the conformational dependence of the electrostatic energy comes from the small variations in the ammonium proton positions and other local electrostatic interactions, such as the C−H$\cdots\pi$ and $\pi-\pi$ interactions. The use of an accurate distributed multipole model for the dominant electrostatic contribution to the lattice energy is thus extremely important for a reliable calculation of the lattice energies.

A more accurate intermolecular potential would include the polarization (induction) energy and charge-transfer energy. However, these may well be relatively constant for the low-energy crystal structures because of the similarity of the packing of the polar groups in all of the hypothetical structures. Another approximation is the assumption that external conditions exist to compensate for the dependence of lattice energy on the morphology in polar crystals.[86] If this is not valid, then for the p-salt, the cell dipole with the experimental molecular conformations is 2.05 e Å, which means that a destabilization term of up to 7.7 kJ mol^{-1} should be added to the lattice energy if we assume a spherical or cubic habit,[87] whereas the known n-salt structures have zero cell dipole moment. A further approximation is that the empirical repulsion−dispersion potential used was fitted to neutral organic crystal structures and heats of sublimation.

Although the solubility ratio is linked to the free energy differences, in this work the relative stability of the hypothetical and known crystal structures was assessed on the basis of the total lattice energies. However, in this case the solution calorimetry and solubility measurements at room temperature (section 3.2.4) show that the very different entropies of n-salt I and the p-salt mean that the free energy and enthalpy stability orders are reversed. Similarly, the enantiotropic relationship between n-salt I and II and the increase of the solubility ratio with increasing temperature[36] are both due to the temperature variation of the entropy. Unfortunately, these critical thermal contributions cannot be estimated within our rigid model. In fact, the MP2/6-31G(d,p) harmonic frequencies for the rotation of the phenyl groups for the in vacuo conformations of the cation and the anion are 43.74 and 45.22 cm^{-1}. The rigid-body ($\mathbf{k} = 0$) harmonic lattice modes are in the ranges 38.4−265.9, 29.1−245.9, and 18.5−247.6 cm^{-1} for the low-temperature p-salt (PMACEP0x), n-salt I (NMACEP02), and n-salt II (NMACEL01), respectively, showing the crystal dynamics cannot be separated into inter- and intramolecular modes. This inadequacy is underlined by the rigid-body vibrational free energies (including zero-point energy) for the p- and n-salt I, estimated from the $k = 0$ modes and elastic constants, being comparable at room temperature.[16]

Even if the free energy difference of diastereomeric salts could be computed at the desired level of accuracy, the design of diastereomeric resolution processes based on the identification of resolving agents that achieve the highest solubility ratio of the diastereomeric pair relies on the assumption that the crystallization is thermodynamically controlled and there is no significant solid solution formation. A further complication may arise from the deviation of the ternary solubility profiles from the ideal behavior, which prohibits the purification beyond the diastereomeric salt ratio at the eutonic point through repeated crystallizations, and hence the separability may not only depend on the physical properties of the isolated diastereomeric salts. Finally, the existence of polymorphs under the same thermodynamic conditions clearly shows that some metastable crystals will be observed because of kinetic factors, which constitutes a major challenge to the field of crystal structure prediction.[88−90] If kinetic factors are important, then the observed resolution efficiency will differ from that theoretically calculated based on simple thermodynamic considerations on the basis of the ternary p-salt, n-salt, and solvent phase diagrams. Thus, even if the theoretical screening of candidate resolving agents based on lattice calculations predicts good separability, this may not be achieved in practice. However, it would be useful in showing which resolving agents satisfy the major thermodynamic separability criteria.

5. Conclusions

The long-anticipated application of crystal structure prediction to screen potential chiral resolving agents for diastereomeric resolution poses a number of challenges to different fields of computational chemistry. We have demonstrated that the use of the experimental information within the CSD can alleviate the search problem and also help focus on the range of molecular conformations that need to be considered. The search with a set of rigid conformations[31] and the estimation of the intramolecular energy with high-level ab initio calculations is an improvement over the often inadequate empirical force fields.[24] Overall, the success of the proposed approach in the reproduction of known forms shows that it is a worthwhile starting point for many types of crystal structure prediction studies, such as pharmaceutical salt selection and modeling of solvates.

However, in this particular case, it is clear that the improvement in obtaining the intramolecular energy from quantum mechanical calculations may be offset by uncertainties in the molecular geometry. Ideally, we would like to refine the low-energy crystal structures and relative energies by balancing the intermolecular packing forces and the intramolecular forces calculated ab initio, as has already been done[28,29] for neutral systems. Although the associated computational cost remains considerable for organic molecules and salts of typical size, a reminimization of the lattice energy with an augmented set of minimization variables that includes all deformable intramolecular torsions and angles is currently underway and will be

reported in a subsequent publication. Nevertheless, although quantitative prediction of the resolution efficiency in the case of the 1-phenylethylammonimum 2-phenylpropanoate has not been obtained within the rigid-body model reported in this paper, the semiquantitative predictions are in good agreement with experiment, and the predictions clearly show that the difference in anion chirality of the p- and n-salts produces very different options for crystallization, consistent with the observed polymorphism of the n-salt.

Thus, although there are many challenges to computational chemistry in improving the relative energies of the known and hypothetical crystal structures of diastereomeric salt pairs, overall, our approach may prove more successful in cases where there is a larger energy difference between the p- and n-salt.[91]

Acknowledgment. The authors acknowledge financial support from the Basic Technology Program of the Research Councils U.K. as part of the CPOSS project (http://www.cposs.org.uk). Thanks are also due to Professor Peter Cains, Mr. Lars Menken, and Ms. Parathy Anandamanoharan for collaborative discussions and provision of experimental data.

Supporting Information Available: Qualitative analysis of ammonium−carboxylate hydrogen bonds, a discussion on the similarities and differences between hypothetical crystal structures, the effect of electron correlation on the intramolecular energy surfaces, and the accuracy of the intermolecular potential model in the reproduction of the ion-pair and hydrogen-bond geometries. This material is available free of charge via the Internet at http://pubs.acs.org.

References and Notes

(1) Kinbara, K.; Tagawa, Y.; Saigo, K. *Tetrahedron: Asymmetry* **2001**, *12*, 2927−2930.

(2) Jacques, J.; Collet, A.; Wilen, S. H. *Enantiomers, Racemates and Resolutions*; Wiley-Interscience: New York, 1981.

(3) Brock, C. P.; Dunitz, J. D. *Chem. Mater.* **1994**, *6*, 1118−1127.

(4) Brock, C. P.; Schweizer, W. B.; Dunitz, J. D. *J. Am. Chem. Soc.* **1991**, *113*, 9811−9820.

(5) Pasteur, L. *C. R. Hebd. Seances Acad. Sci.* **1853**, *37*, 162.

(6) Wood, W. M. L. Crystal Science Techniques in the Manufacture of Chiral Compounds. In *Chirality in Industry II*; Collins, N. A., Sheldrake, G. N., Crosby, J., Eds.; Wiley & Sons: New York, 1997.

(7) Collet, A. *Angew. Chem., Int. Ed.* **1998**, *37*, 3239−3241.

(8) Collet, A. In *Comprehensive Supramolecular Chemistry*; Atwood, J. L., Davies, J. E. D., MacNicol, D. D., Reinhoudt, D. N., Eds.; Pergammon: Oxford, U.K., 1996; pp 113−149.

(9) Osborne, D. A.; Dreher, W. R., Jr.; Gore, H. R., Jr.; Stoddard, A.; Valente, E. J. *J. Chem. Crystallogr.* **2000**, *30*, 583−588.

(10) Pallavicini, M.; Bolchi, C.; Moroni, B.; Valoti, E.; Piccolo, O. *Tetrahedron: Asymmetry* **2003**, *14*, 2247−2251.

(11) Bolchi, C.; Fumagalli, L.; Moroni, B.; Pallavicini, M.; Valoti, E. *Tetrahedron: Asymmetry* **2003**, *14*, 3779−3785.

(12) Pallavicini, M.; Bolchi, C.; Fumagalli, L.; Valoti, E.; Villa, L. *Tetrahedron: Asymmetry* **2002**, *13*, 2277−2282.

(13) Sakurai, R.; Sakai, K. *Tetrahedron: Asymmetry* **2003**, *14*, 411−413.

(14) Leusen, F. J. J.; Noordik, J. H.; Karfunkel, H. R. *Tetrahedron* **1993**, *49*, 5377−5396.

(15) Price, S. L. *CrystEngComm* **2004**, *6*, 344−353.

(16) Day, G. M.; Price, S. L.; Leslie, M. *J. Phys. Chem. B* **2003**, *107*, 10919−10933.

(17) Van Eijck, B. P. *J. Comput. Chem.* **2001**, *22*, 816−826.

(18) Lommerse, J. P. M.; Motherwell, W. D. S.; Ammon, H. L.; Dunitz, J. D.; Gavezzotti, A.; Hofmann, D. W. M.; Leusen, F. J. J.; Mooij, W. T. M.; Price, S. L.; Schweizer, B.; Schmidt, M. U.; Van Eijck, B. P.; Verwer, P.; Williams, D. E. *Acta Crystallogr., Sect. B: Struct. Sci.* **2000**, *56*, 697−714.

(19) Motherwell, W. D. S.; Ammon, H. L.; Dunitz, J. D.; Dzyabchenko, A.; Erk, P.; Gavezzotti, A.; Hofmann, D. W. M.; Leusen, F. J. J.; Lommerse, J. P. M.; Mooij, W. T. M.; Price, S. L.; Scheraga, H.; Schweizer, B.; Schmidt, M. U.; Van Eijck, B. P.; Verwer, P.; Williams, D. E. *Acta Crystallogr., Sect. B: Struct. Sci.* **2002**, *58*, 647−661.

(20) Leusen, F. J. J.; Slot, H. J. B.; Noordik, J. H.; van der Haest, A. D.; Wynberg, H.; Bruggink, A. *Recl. Trav. Chim. Pays−Bas* **1992**, *111*, 111−118.

(21) Leusen, F. J. J. *Cryst. Growth Des.* **2003**, *3*, 189−192.

(22) McArdle, P.; Gilligan, K.; Cunningham, D.; Dark, R.; Mahon, M. *CrystEngComm* **2004**, *6*, 303−309.

(23) Gervais, C.; Grimbergen, R. F. P.; Markovits, I.; Ariaans, G. J. A.; Kaptein, B.; Bruggink, A.; Broxterman, Q. B. *J. Am. Chem. Soc.* **2004**, *126*, 655−662.

(24) Brodersen, S.; Wilke, S.; Leusen, F. J. J.; Engel, G. *Phys. Chem. Chem. Phys.* **2003**, *5*, 4923−4931.

(25) Breu, J.; Domel, H.; Norrby, P. O. *Eur. J. Inorg. Chem.* **2000**, 2409−2419.

(26) Mooij, W. T. M.; van Dunijneveldt, F. B.; van Duijneveldt-van de Rijdt, J. G. C. M.; Van Eijck, B. P. *J. Phys. Chem. A* **1999**, *103*, 9872−9882.

(27) Mooij, W. T. M.; Van Eijck, B. P.; Kroon, J. *J. Phys. Chem. A* **1999**, *103*, 9883−9890.

(28) Van Eijck, B. P.; Mooij, W. T. M.; Kroon, J. *J. Comput. Chem.* **2001**, *22*, 805−815.

(29) Van Eijck, B. P.; Mooij, W. T. M.; Kroon, J. *J. Phys. Chem. B* **2001**, *105*, 10573−10578.

(30) Allen, F. H. *Acta Crystallogr., Sect. B: Struct. Sci.* **2002**, *58*, 380−388.

(31) Ouvrard, C.; Price, S. L. *Cryst. Growth Des.* **2004**, *4*, 1119−1127.

(32) Van Eijck, B. P. *J. Comput. Chem.* **2002**, *23*, 456−462.

(33) Verwer, P.; Leusen, F. J. J. Computer Simulation to Predict Possible Crystal Polymorphs. In *Reviews in Computational Chemistry*; Lipkowitz, K. B., Boyd, D. B., Eds.; Wiley-VCH: New York, 1998; pp 327−365.

(34) Brianso, M. C. *Acta Crystallogr., Sect. B: Struct. Crystallogr. Cryst. Chem.* **1976**, *32*, 3040−3045.

(35) Menken, L.; Tocher, D. A.; Cains, P. W., to be sumbitted for publication.

(36) Leclercq, M.; Jacques, J. *Bull. Soc. Chim. Fr. II-Ch.* **1975**, 2052−2056.

(37) Dufour, F.; Gervais, C.; Petit, M. N.; Perez, G.; Coquerel, G. *J. Chem. Soc., Perkin Trans. 2* **2001**, 2022−2036.

(38) Dufour, F.; Perez, G.; Coquerel, G. *Bull. Chem. Soc. Jpn.* **2004**, *77*, 79−86.

(39) Frisch, M. J.; Trucks, G. W.; Schlegel, H. B.; Scuseria, G. E.; Robb, M. A.; Cheeseman, J. R.; Zakrzewski, V. G.; Montgomery, J. A., Jr.; Stratmann, R. E.; Burant, J. C.; Dapprich, S.; Millam, J. M.; Daniels, A. D.; Kudin, K. N.; Strain, M. C.; Farkas, O.; Tomasi, J.; Barone, V.; Cossi, M.; Cammi, R.; Mennucci, B.; Pomelli, C.; Adamo, C.; Clifford, S.; Ochterski, J.; Petersson, G. A.; Ayala, P. Y.; Cui, Q.; Morokuma, K.; Malick, D. K.; Rabuck, A. D.; Raghavachari, K.; Foresman, J. B.; Cioslowski, J.; Ortiz, J. V.; Stefanov, B. B.; Liu, G.; Liashenko, A.; Piskorz, P.; Komaromi, I.; Gomperts, R.; Martin, R. L.; Fox, D. J.; Keith, T.; Al-Laham, M. A.; Peng, C. Y.; Nanayakkara, A.; Gonzalez, C.; Challacombe, M.; Gill, P. M. W.; Johnson, B. G.; Chen, W.; Wong, M. W.; Andres, J. L.; Head-Gordon, M.; Replogle, E. S.; Pople, J. A. *Gaussian 98*, revision A.9; Gaussian, Inc.: Pittsburgh, PA, 1998.

(40) Bruno, I. J.; Cole, J. C.; Kessler, M.; Luo, J.; Motherwell, W. D. S.; Purkis, L. H.; Smith, B. R.; Taylor, R.; Cooper, R. I.; Harris, S. E.; Orpen, A. G. *J. Chem. Inf. Comput. Sci.* **2004**, *44*, 2133−2144.

(41) Holden, J. R.; Du, Z. Y.; Ammon, H. L. *J. Comput. Chem.* **1993**, *14*, 422−437.

(42) Brock, C. P.; Dunitz, J. D. *Mol. Cryst. Liq. Cryst. Sci. Technol., Sect. A* **1994**, *242*, 61−69.

(43) Wilson, A. J. C. *Acta Crystallogr., Sect. A: Found. Crystallogr.* **1993**, *49*, 795−806.

(44) Butchart, B.; Chapman, C.; Emmerich, W. In *Proceedings of the U.K. e-Science All Hands Meeting*; Cox, S. J. Ed.; EPSRC, Swindon, U.K., 2003.

(45) Cox, S. R.; Hsu, L. Y.; Williams, D. E. *Acta Crystallogr., Sect. A: Cryst. Phys., Diffr., Theor. Gen. Crystallogr.* **1981**, *37*, 293−301.

(46) Williams, D. E.; Cox, S. R. *Acta Crystallogr., Sect. B: Struct. Sci.* **1984**, *40*, 404−417.

(47) Coombes, D. S.; Price, S. L.; Willock, D. J.; Leslie, M. *J. Phys. Chem.* **1996**, *100*, 7352−7360.

(48) Stone, A. J.; Alderton, M. *Mol. Phys.* **1985**, *56*, 1047−1064.

(49) Stone, A. J. *GDMA: A Program for Performing Distributed Multipole Analysis of Wave Functions Calculated Using the Gaussian Program System*, version 1.0; University of Cambridge: Cambridge, U.K., 1999.

(50) Ewald, P. *Ann. Phys.* **1921**, *64*, 253.

(51) Willock, D. J.; Price, S. L.; Leslie, M.; Catlow, C. R. A. *J. Comput. Chem.* **1995**, *16*, 628−647.

(52) Krivy, I.; Gruber, B. *Acta Crystallogr., Sect. A: Cryst. Phys., Diffr., Theor. Gen. Crystallogr.* **1976**, *32*, 297−298.

(53) Giacovazzo, C.; Monaco, H. L.; Artioli, G.; Viterbo, D.; Ferraris, G.; Gilli, G.; Zanotti, G.; Catti, M. *Fundamentals of Crystallography*; Oxford Science Publications: Oxford, U.K., 2002.

(54) Santoro, A.; Mighell, A. D. *Acta Crystallogr., Sect. A: Cryst. Phys., Diffr., Theor. Gen. Crystallogr.* **1970**, *26*, 124−127.
(55) Gruber, B. *Acta Crystallogr., Sect. A: Found. Crystallogr.* **1989**, *45*, 123−131.
(56) Spek, A. L. *PLATON, A Multipurpose Crystallographic Tool*; Utrecht University: Utrecht, The Netherlands, 2003.
(57) De Gelder, R.; Wehrens, R.; Hageman, J. A. *J. Comput. Chem.* **2001**, *22*, 273−289.
(58) Chisholm, J. A.; Motherwell, S. *J. Appl. Crystallogr.* **2005**, *38*, 228−231.
(59) Van Eijck, B. P.; Kroon, J. *J. Comput. Chem.* **1997**, *18*, 1036−1042.
(60) Bruno, I. J.; Cole, J. C.; Edgington, P. R.; Kessler, M.; Macrae, C. F.; McCabe, P.; Pearson, J.; Taylor, R. *Acta Crystallogr., Sect. B: Struct. Sci.* **2002**, *58*, 389−397.
(61) Etter, M. C. *Acc. Chem. Res.* **1990**, *23*, 120−126.
(62) Etter, M. C.; MacDonald, J. C.; Bernstein, J. *Acta Crystallogr., Sect. B: Struct. Sci.* **1990**, *46*, 256−262.
(63) Reiling, S.; Brickmann, J.; Schlenkrich, M.; Bopp, P. A. *J. Comput. Chem.* **1996**, *17*, 133−147.
(64) Frisch, M. J.; DelBene, J. E.; Binkley, J. S.; Schaefer, H. F. *J. Chem. Phys.* **1986**, *84*, 2279−2289.
(65) Allen, F. H.; Harris, S. E.; Taylor, R. *J. Comput.-Aided Mol. Des.* **1996**, *10*, 247−254.
(66) Larsen, S.; Kozma, D.; Acs, M. *Acta Chem. Scand.* **1994**, *48*, 32−36.
(67) Allen, F. H.; Kennard, O.; Watson, D. G. *J. Chem. Soc., Perkin Trans. 2* **1987**, S1−S19.
(68) Taylor, R.; Kennard, O. *Acta Crystallogr., Sect B: Struct. Sci.* **1983**, *39*, 133−138.
(69) Speakman, J. C. In *Molecular Structure by Diffraction Methods*; Sim, G. A., Sutton, L. E., Eds.; The Chemical Society: London, U.K., 1973; p 203.
(70) Cruickshank, D. W. J. *Acta Crystallogr.* **1956**, *9*, 757−758.
(71) The neutron standard N−H bond length (CSD September 1987, Allen et al. 1987) is 1.009 Å for three-coordinate nitrogen atoms. For four-coordinate nitrogen atoms (X_3-N^+-H), it is increased to 1.036 Å with 25% of the observations being larger than 1.045 Å. In this work, we employed a 1.01 Å standard N−H length. Although a sligthly higher value may be more appropriate, the variation in the experimental N−H bond lengths suggests that no significant improvements can be expected within our rigid-body model.
(72) Williams, D. E. *J. Mol. Struct.* **1999**, *486*, 321−347.
(73) Beyer, T.; Price, S. L. *CrystEngComm* **2000**, 183−190.
(74) Burger, A.; Ramberger, R. *Microchim. Acta* **1979**, 259−271.
(75) Burger, A.; Ramberger, R. *Microchim. Acta* **1979**, 273−316.
(76) Yff, B.; Menken, L.; Royall, P. G.; Cains, P. W., to be submitted for publication.
(77) Bruno, I. J.; Cole, J. C.; Lommerse, J. P. M.; Rowland, R. S.; Taylor, R.; Verdonk, M. L. *J. Comput.-Aided Mol. Des.* **1997**, *11*, 525−537.
(78) Berman, H. M.; Westbrook, J.; Feng, Z.; Gilliland, G.; Bhat, T. N.; Weissig, H.; Shindyalov, I. N.; Bourne, P. E. *Nucleic Acids Res.* **2000**, *28*, 235−242.
(79) Berman, H. M.; Battistuz, T.; Bhat, T. N.; Bluhm, W. F.; Bourne, P. E.; Burkhardt, K.; Feng, Z.; Gilliland, G. L.; Lype, L.; Jain, S.; Fagan, P.; Marvin, J.; Padilla, D.; Ravichandran, V.; Schneiner, B.; Thanki, N.; Weissig, H.; Westbrook, J. D.; Zardecki, C. *Acta Crystallogr., Sect. D: Biol. Crystallogr.* **2002**, *58*, 899−907.
(80) Desiraju, G. R. *Acc. Chem. Res.* **2002**, *35*, 565−573.
(81) Taylor, R.; Kennard, O.; Versichel, W. *Acta Crystallogr., Sect. B: Struct. Sci.* **1984**, *40*, 280−288.
(82) Taylor, R.; Kennard, O.; Versichel, W. *J. Am. Chem. Soc.* **1983**, *105*, 5761−5766.
(83) Karamertzanis, P. G.; Pantelides, C. C. *J. Comput. Chem.* **2005**, *26*, 304−324.
(84) Nowell, H.; Price, S. L. *Acta Crystallogr., Sect. B: Struct. Sci.*, in press.
(85) Nowell, H.; Frampton, C. S.; Price, S. L., submitted for publication.
(86) Van Eijck, B. P.; Kroon, J. *J. Phys. Chem. B* **1997**, *101*, 1096−1100.
(87) Smith, E. R. *Proc. R. Soc. London, Ser. A* **1981**, *375*, 475−505.
(88) Davey, R. J.; Allen, K.; Blagden, N.; Cross, W. I.; Lieberman, H. F.; Quayle, M. J.; Righini, S.; Seton, L.; Tiddy, G. J. T. *CrystEngComm* **2002**, 257−264.
(89) Bernstein, J.; Davey, R. J.; Henck, J. O. *Angew. Chem., Int. Ed.* **1999**, *38*, 3441−3461.
(90) Price, S. L. *Adv. Drug Delivery Rev.* **2004**, *56*, 301−319.
(91) Yoshioka, R.; Hiramatsu, H.; Okamura, K.; Tsujioka, I.; Yamada, S. *J. Chem. Soc., Perkin Trans 2* **2000**, 2121−2128.
(92) Filippini, G.; Gavezzotti, A. *Acta Crystallogr., Sect. B: Struct. Sci.* **1993**, *49*, 868−880.
(93) Hofmann, D. W. M. *Acta Crystallogr., Sect B: Struct. Sci.* **2002**, *58*, 489−493.
(94) To define the torsion angles uniquely, the following conventions were made: C1 and C5 were selected as the phenyl carbons that give a positive sign for the torsion angles θ_1 and θ_3, respectively, O1 was selected as the carboxylate oxygen that gives a negative sign for the torsion θ_2, and H1 was selected as the ammonium hydrogen that gives a torsion angle θ_4 between −120° and 0°. These conventions refer to (*R*)-2-phenylpropanoate and (*R*)-1-phenylethylammonium, and the signs of the torsions are inverted to refer to their chiral ions.
(95) Kroon, J.; Kanters, J. A.; van Duijneveldt-van de Rijdt, J. G. C. M.; van Dunijneveldt, F. B.; Vliegenthart, J. A. *J. Mol. Struct.* **1975**, *24*, 109−129.